Clim Dyn
DOI 10.1007/s00382-016-3360-8

July 2017, Volume 49, Issue 1–2, pp 595–618

Coherency of late Holocene European speleothem $\delta^{18}O$ records linked to North Atlantic Ocean circulation

Michael Deininger[1] · Frank McDermott[1,2] · Manfred Mudelsee[3,4] · Martin Werner[4] · Norbert Frank[5] · Augusto Mangini[5]

Received: 10 June 2016 / Accepted: 9 September 2016

Abstract Speleothem $\delta^{18}O$ records provide valuable information about past continental environmental and climatic conditions, although their interpretation is often not straightforward. Here we evaluate a compilation of late Holocene speleothem $\delta^{18}O$ records using a Monte Carlo based Principal Component Analysis (MC-PCA) method that accounts for uncertainties in individual speleothem age models and for the variable temporal resolution of each $\delta^{18}O$ record. The MC-PCA approach permits not only the identification of temporally coherent changes in speleothem $\delta^{18}O$; it also facilitates their graphical depiction and evaluation of their spatial coherency. The MC-PCA method was applied to 11 Holocene speleothem $\delta^{18}O$ records that span most of the European continent (apart from the circum-Mediterranean region). We observe a common (shared) mode of speleothem $\delta^{18}O$ variability that suggests millennial-scale coherency and cyclicity during the last 4.5 ka. These changes are likely caused by variability in atmospheric circulation akin to that associated with the North Atlantic Oscillation, reflecting meridionally shifted westerlies. We argue that these common large-scale variations in European speleothem $\delta^{18}O$ records are in phase with changes in the North Atlantic Ocean circulation indicated by the vigour of the Iceland Scotland Overflow Water (ISOW), the strength of the subpolar gyre (SPG) and an ocean stacked North Atlantic ice rafted debris (IRD) index. Based on a recent modelling study, we conclude that these changes in the North Atlantic circulation history may be caused by wind stress on the ocean surface driven by shifted westerlies. However, the mechanisms that ultimately force the westerlies remain unclear.

Keywords Speleothems · Spatio-temporal coherency · Palaeoclimate dynamics · Subpolar gyre · ISOW · Westerlies

Electronic supplementary material The online version of this article (doi:10.1007/s00382-016-3360-8) contains supplementary material, which is available to authorized users.

✉ Michael Deininger
michael.deininger@ucd.ie

[1] UCD School of Earth Sciences, University College Dublin, Belfield, Dublin 4, Ireland

[2] UCD Earth Institute, University College Dublin, Belfield, Dublin 4, Ireland

[3] Climate Risk Analysis, Kreuzstrasse 27, Heckenbeck, 37581 Bad Gandersheim, Germany

[4] Alfred Wegener Institute, Helmholtz Centre for Polar and Marine Research, Bussestraße 24, 27570 Bremerhaven, Germany

[5] Institute of Environmental Physics, Heidelberg University, Im Neuenheimer Feld 229, 69120 Heidelberg, Germany

1 Introduction

Speleothems are valuable archives of past climatic conditions on the continents. Major strengths include their suitability for accurate U-series age determinations (e.g. Cheng et al. 2013; Hoffmann et al. 2007; Richards and Dorale 2003) and their preservation of multiple quasi-independent climate proxies, e.g., mineralogy, textural features, stable isotopes, trace elements (Fairchild et al. 2006; Fairchild and Treble 2009; Frisia et al. 2000; McDermott 2004). However, the interpretation of some key geochemical parameters (e.g. $\delta^{18}O$) can sometimes be ambiguous, because several processes influence the transport and cycling of oxygen isotopes, as well as their incorporation into speleothem carbonate (e.g. Lachniet 2009). In order to better

understand the predominant processes that control oxygen isotope variations, forward models have been developed to simulate the effects of various processes on the speleothem climate proxies (e.g. Baker et al. 1998; Deininger et al. 2012; Dreybrodt and Scholz 2011). Furthermore, isotope enabled general circulation models (e.g. ECHAM5-wiso) help us to understand the $\delta^{18}O$ variability in precipitation that in turn can be captured by speleothems (e.g. Dietrich et al. 2013; Jex et al. 2013; Langebroek et al. 2011; Lohmann et al. 2013; Werner et al. 2011). Laboratory and field experiments have also advanced our understanding of the processes that determine speleothem $\delta^{18}O$ values (and other climate proxies) (e.g. Day and Henderson 2011; Hartland et al. 2012; Huang and Fairchild 2001; Polag et al. 2010; Riechelmann et al. 2013; Tremaine et al. 2011). While much progress has been made, it often remains challenging to distinguish between local, regional and meso- to large-scale climate signatures within individual speleothem $\delta^{18}O$ records.

A promising approach to advance our understanding of large-scale climate signals is through the use of compilations from several coeval speleothems on a regional scale (Lachniet et al. 2007; McDermott et al. 2011). Our study builds on the initial work of McDermott et al. (2011) on the scale of the European continent, but explicitly takes age model uncertainties into account and applies Principal Component Analysis (PCA) to retrieve quantitative measures of regional coherence and associated uncertainties. Recent studies have also used other methods to analyse compilations of multiple speleothems using inter-system recurrence networks (Feldhoff et al. 2012), network analysis (Rehfeld et al. 2013) and predictable components (Fischer 2016). The PCA methods employed in this study offer a powerful tool to investigate the spatio-temporal coherency (e.g. Preisendorfer 1988) of numerous meteorological observations (e.g. sea level pressure) (e.g. Wallace and Gutzler 1981) and have also found use in palaeoclimatology (e.g. Anchukaitis and Tierney 2012; Mann et al. 1998). Nonetheless, the use of PCA methods in palaeoclimatology is not straightforward, because palaeoclimate proxies present particular technical challenges including the age uncertainties that result from the dating techniques (e.g. U-series disequilibrium methods) and the variable temporal resolutions of the proxy records (resulting from variable growth rates). Here we take steps to overcome these obstacles, and then apply PCA methods to a unique compilation of European speleothem oxygen isotope ($\delta^{18}O$) datasets, ultimately to test the spatio-temporal coherency of these observations during the last 5 ka. Though some of the selected speleothem $\delta^{18}O$ records cover the entire Holocene, we restrict our analysis to the last 5 ka, the common growth period for all the analysed speleothems. Europe is a key-region to test PCA on speleothems because the spatial density of speleothem $\delta^{18}O$ datasets is highest worldwide. It is also a region with strong present day spatial climate patterns such as the North Atlantic Oscillation (NAO) that impacts temperature, precipitation (Hurrell 1995) and precipitation $\delta^{18}O$ patterns, especially during the winter months (Baldini et al. 2008; Langebroek et al. 2011). Furthermore, the European climate is also closely linked to the North Atlantic Ocean circulation and common modes of proxy-climate variability can yield insights into palaeoclimate dynamics.

Our approach demonstrates the existence of coherent spatio-temporal variations in European speleothem $\delta^{18}O$ records, verifying that at least during the last 5 ka, speleothem $\delta^{18}O$-values successfully capture meso- to large-scale climate variability. Furthermore, we show that this coherent climate signal is broadly in phase with previously documented variations of North Atlantic Ocean circulation, suggesting a common mode for the late Holocene continental and oceanic climate variability.

2 Methods

For the investigation of lacustrine records from East Africa, Anchukaitis and Tierney (2012) used an advanced PCA approach, taking the age uncertainty of each record into account using a Monte Carlo simulation (MC-PCA). This is important, because as a consequence of age uncertainties in dating techniques (e.g. speleothem U-series ages) the climate-proxy records can be shifted in time within these uncertainties. Hence, every climate-proxy record can in principle be stretched and compressed within some limits defined by the age uncertainties. This issue becomes critical when compilations of climate-proxy datasets are compared with each other, or analysed with statistical methods (as is done here), because in principle the climate-proxy datasets could be deliberately shifted in time until, for example, a maximum correlation between all datasets is reached; or in other words, until the differences between records are minimized. However, this approach would require a priori assumptions about signal coherence and is therefore avoided in this study. For this reason we adopted the Monte Carlo approach of Anchukaitis and Tierney (2012). However, we have additionally modified their method to take account of the typically variable temporal resolution of speleothem $\delta^{18}O$ record observations.

For a discussion of the basic principles of PCA we refer the reader to the accompanying supplementary information. To perform PCA on a compilation of palaeoclimate datasets (e.g. speleothem $\delta^{18}O$ records), observations should be equally spaced in time. However, this precondition is rarely met in the case of speleothem data and indeed for most palaeoclimate archives. Speleothem growth rates are variable (e.g. Baker et al. 1998; McDermott et al. 1999) leading to

irregular time spacing when the normal strategy of sampling for isotope analysis at equal distances along a speleothem growth axis is followed (Spötl and Mattey 2006). Annually-layered speleothems are exceptions, because in these relatively rare cases it is may be possible to ascribe a measured proxy value (e.g. $\delta^{18}O$) to a certain year (e.g. Baker et al. 2011). To account for these properties, a routine, which accounts for different temporal resolutions of speleothem proxy records and for age uncertainties of each speleothem was developed using a Monte Carlo simulation, hereafter referred to as MC-PCA.

2.1 Routine of the MC-PCA

2.1.1 Routine for MC-PCA accounting for different temporal resolutions and age uncertainties

The PCA routine is performed in four steps:

Step 1: Accounting for the age uncertainty of each speleothem age model: To account for age uncertainty, a Monte Carlo approach is used to allow each age to vary within its 1-sigma uncertainty (assuming a Gaussian distribution), resulting in a "new" age model for every speleothem in the compilation. To avoid age-inversions, the age-model's youngest age is set as the starting age, and all subsequent U-series ages are required to be in stratigraphic order. For this, the routine first calculates the youngest age (1st age) of the respective speleothem age model. Subsequently, the 2nd age is calculated, and so on until the last age of the age model is calculated. Assuming a compilation of *m* speleothems, this results in *m* "new" age models. These age models are referred to hereafter as the "new age models".

Step 2: Calculation of the climate-proxy record using the new age model: To calculate the climate-proxy-age relation, we assume a linear interpolation between the ages of the new age model. This "simplistic" assumption has also been made for other algorithms to calculate speleothem age models (e.g. Scholz and Hoffmann 2011). This approach results in *m* "new" climate-proxy records, all of which typically have different temporal resolutions (here we use "temporal resolution" to refer to timing between two adjacent samples). In the following, the new calculated climate-proxy age-depth relations are denoted by "new climate-proxy records".

Step 3: Equalising and temporal upscaling of climate-proxy resolution of the new records: To ensure that all new climate-proxy records of the speleothem compilation have the same temporal resolution, a resampling protocol is applied that accounts for different temporal resolutions of the new climate-proxy records. For this the resampling procedure upscales the new climate-proxy records in time to ensure that no new information is generated (unlike temporal downscaling). In the following, we refer to the climate-proxy records after resampling (i.e. upscaling) as "upscaled climate-proxy records". The upscaling is achieved as follows. Assuming a compilation of *m* speleothems, the algorithm determines the overlapping growth history of these *m* speleothems. Subsequently, this period is subdivided into 30-year long bins, i.e., to a temporal resolution of 30 years. (This temporal resolution is our precondition to the used speleothem climate-proxy time series and, therefore, no speleothems whose temporal resolution is lower than 30 years are used.) For every bin, the average climate-proxy value is calculated using a Gaussian kernel (as described by Rehfeld et al. 2011) applied to all climate-proxy values within the respective bin ($\sigma = 6.37$ years). Hence for the calculation of the average value all climate-proxy values that are located within ± 15 years from the centre age of the bin are considered and weighted with respect to their distance from the centre age whereas proxy values that are closer to centre bin a more weighed. The Gaussian kernel method is identified to be very suitable for irregularly spaced palaeoclimate datasets by Rehfeld et al. (2011). This procedure results in *m* upscaled climate-proxy records, which have the same temporal resolution and span the same time period.

Step 4: Performing of Principal Component Analysis on the compilation of upscaled climate-proxy records: Before the PCA is applied to the upscaled climate-proxy records, all climate-proxy records are normalised to a mean value of 0 and a standard deviation of 1. No further data processing was applied. Depending on the number of analysed speleothems, e.g., *m*, this results in *m* Eigenvalues, *m* Principal Components (PCs) and *m*m* loadings, where the PC with the highest eigenvalue, the 1st PC, explains most of the variance (referred as total explained variance) of the entire compilation. The loading between a speleothem $\delta^{18}O$ record and a PC is a value that expresses the strength of the coupling of the speleothem $\delta^{18}O$ record to the common mode of variability expressed by the respective PC. The pattern that results from the spatial visualisation of the loadings is referred to here as the spatio-temporal pattern.

2.1.2 Monte Carlo approach for the Principal Component Analysis (MC-PCA)

To account for the age uncertainty, Steps 1 to 4 are repeated 2000 times. This number is based on an analysis of how fast the mean eigenvalues and their respective variance converge to a stable value (Deininger 2013). In every run, a new age model is calculated (Step 1), which results in new upscaled climate-proxy records (Step 2 and 3). Finally, the upscaled climate-proxy records are analysed using PCA (Step 4). Assuming that Steps 1 to 4 are repeated n-times, this results in m*n eigenvalues and PCs, respectively, and m*m*n loadings, which can be analysed to evaluate the

spatio-temporal coherency of the compiled speleothem climate-proxy records. To calculate the mean value of each individual PC, the time covered by all PCs is subdivided into 30-year bins. For every bin, the arithmetic mean is calculated by considering only those PC values (of all MC simulations) that are within the respective bin. This mean value is assigned to the centre age of each bin. Furthermore, the respective standard deviation of the mean value is calculated. Hence, the mean PC has a constant temporal resolution of 30 years. Furthermore, the mean eigenvalue of a PC is calculated by the arithmetic mean of all eigenvalues derived by the PCA. The mean loading between the speleothem $\delta^{18}O$ records and a PC is the median calculated from all received loadings.

2.2 Effects of age uncertainties

Age uncertainties can cause a "flipping-effect" of the PCs depending on the magnitude of the uncertainties (Figure S1a), which results in a bimodal distribution of the loadings of single speleothems (Figure S2). However, this effect does not impose limitations on the interpretation of the results of MC-PCA of speleothem compilations, because the results can be corrected for the flipping effect (see supplementary information S1). Another effect of the age uncertainties is that the PCs are smoothed, depending, again, on the magnitude of the age uncertainties (Figure S1b). However, this effect is likely to be negligible if only a small number of speleothems from the compilation has large age uncertainties. Further details on both aspects of the data treatment are found in Supplement S1.

2.3 Selection rules for principal components

To select the dominant PCs, which are likely to be meaningful in terms of total explained variance or by being distinguishable from white noise, various criteria can be applied. Common criteria are that eigenvalues have to be greater than unity (Kaiser 1960) or a scree plot can be used to identify meaningful PCs by evaluating the slope (Cattell 1966). Furthermore, North et al. (1982) developed a "rule of thumb" to select PCs based on an estimate of the sampling error for the eigenvalues. However, more rigorous approaches are described by Preisendorfer (1988) based on Monte Carlo approaches: these selection rules are based on the one hand by evaluating the total explained variance against an appropriate null hypothesis, usually using white and red noise models (dominant variance rule) or on the other hand by testing the whiteness of each principal component (time history rule). However, it is important to note that it is not the physical meaning of the PCs that is tested, but rather if the variance or persistence properties of a PC withstand certain null hypotheses.

Preisendorfer (1988) pointed out that dominant variance rules might not always be appropriate for selecting PCs. This is because some common modes recorded in the compilation might not be of dominant variance. This might be certainly the case for speleothem $\delta^{18}O$ compilations where several processes can modify the ultimately recorded $\delta^{18}O$ signal (Deininger et al. 2012; Lachniet 2009; McDermott 2004), even if the records investigated are part of the same hydrological cycle as it is the case for this study. In addition, a test with the isotope enabled General Circulation Model ECHAM5-wiso (Langebroek et al. 2011; Werner et al. 2011), shows that dominant mode driving modern winter (October–March) precipitation-weighted precipitation $\delta^{18}O$ signals accounts for about 27.6 % of the variance (see Sect. 4). Hence, dominant variance rules applied to speleothem $\delta^{18}O$ datasets might underestimate the number of potentially meaningful PCs. Preisendorfer (1988) suggested to apply time history rules instead of using dominant variance rules. For this reason, we use only the most dominant PC, identified to be "potentially meaningful" by Rule KS2. For Rule KS2, the 95 % level of the Kolmogorov–Smirnov (KS) test (d_{95} value) is used as a selection rule and the average d value of a PC must be above this level to be selected as potentially meaningful. The 95 % confidence levels of the white and red noise model of Rule N are used to better assess the strength of the common mode. These tests are further explained in Section S3.1 (Rule KS2) and S3.2 (Rule N).

An example of the application of these selection rules is illustrated in Fig. 1 for two investigated speleothem $\delta^{18}O$ compilations: compilation 5k comprises six speleothem $\delta^{18}O$ records (which cover the time period 0.1–5 ka BP) and compilation 1k.VIII, comprises seven speleothem $\delta^{18}O$ records (which span the period from 0.01–1 ka BP). A detailed explanation on all compilations and the analysed speleothem $\delta^{18}O$ datasets is given in the following section. Rule KS2 and Rule N (white noise null model) indicates for compilation 5k (compilation 1k.VIII) that all six (1st–4th PC) and the 1st PC (1st–2nd PC) are potentially meaningful on a 95 % confidence level, respectively. Furthermore, Rule N (red noise null model) shows that the 1st PC of compilation 1k.VIII exceeds the 95 % confidence level, indicating a particularly dominant mode of the 1st PC. For these compilations the 1st PCs are interpreted as potentially meaningful and are compared to other palaeoclimate datasets.

3 Data compilation

For this MC-PCA based study, well-characterised European speleothems are used that fulfil quality criteria with regards to the age accuracy and temporal resolution. These

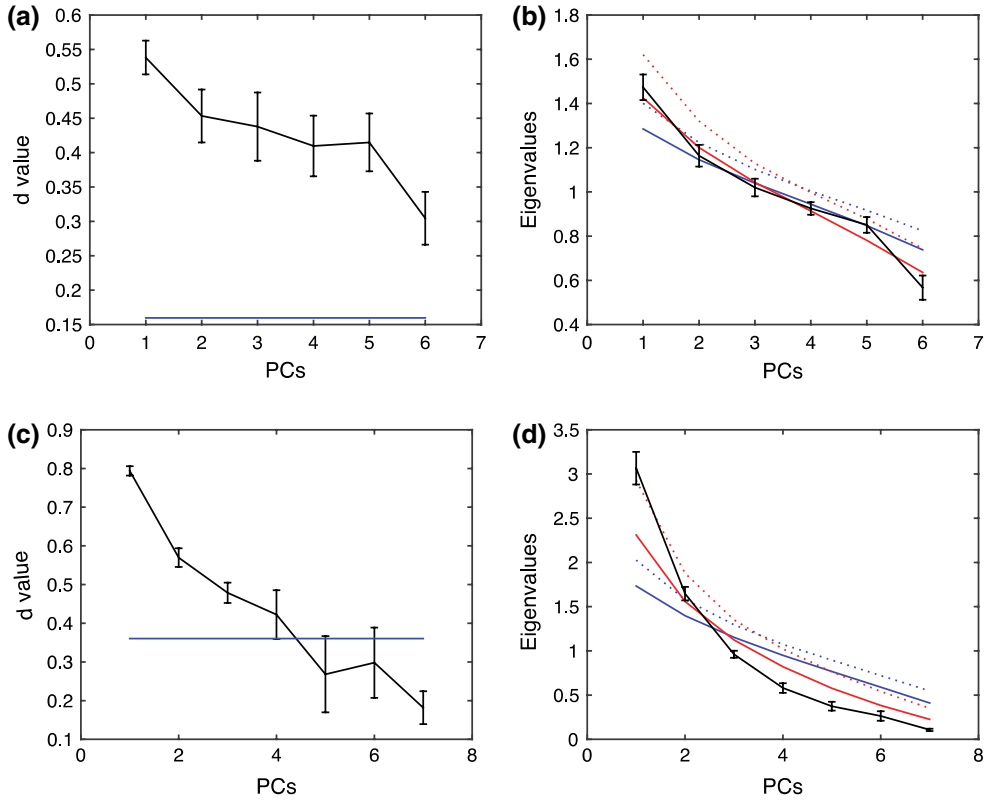

Fig. 1 The panels on the *left hand side* show the results of Rule KS2; those on the *right hand side* show the results of Rule N for compilation 5k (**a**, **b**) and compilation 1k.VIII (**c**, **d**). The panels of Rule KS2 (**a**, **c**) show the average d values (*black*) and its 1-sigma standard deviation for every principal component; the blue line indicates the 95 % significance level of the Kolmogorov–Smirnov test. The mean d value is calculated from a total of 2000 Monte Carlo simulations. The panels of Rule N (**b**, **d**) show the eigenvalues for every principal component of the conducted MC-PCA. The *black line* indicates the mean eigenvalue of the respective compilation of speleothem $\delta^{18}O$ records including the 1-sigma standard deviation from the mean based on a total of 2000 Monte Carlo simulations using MC-PCA. The *blue* and *red dashed line* illustrated the 95 % confidence level of the white noise and red noise (AR-1) null model, respectively. The *solid lines* indicate the mean value for PC for the respective null model

criteria are: (i) that the speleothems have been U-series dated by either thermal ionization mass spectrometry (TIMS), by inductively coupled plasma mass spectrometry (ICP-MS) to have small age-uncertainties or well constrained age models by lamina counting and (ii) that the temporal resolution of the climate-proxy dataset employed is better than 30 years. Criterion (ii) is necessary because of the applied temporal upscaling to 30 years (Step 3 in 2.1.1). $\delta^{18}O$ is used here as the climate-proxy, although in principle the approach can be applied to any other climate-sensitive proxy (e.g. $\delta^{13}C$) in speleothems or other archives. The $\delta^{18}O$ signal imprinted in European speleothems is mainly a proxy for winter climate, because most of the water is infiltrated into the karst system during this period. The speleothem records investigated here are listed in Table 1 and their geographical distribution is illustrated in Fig. 2.

Geographically, the compilation covers areas stretching from Northern- and Central-Europe, to the western margin of the European continent, to northern Turkey and the northern Levant. The temporal coverage is densest in the late Holocene, in particular for the last 5 ka. Six speleothems cover the entire last 5 ka (BU-4, CC-3, FM-3, GAR-01, SO-1 and SPA-12), allowing analysis of spatio-temporal coherence over this time. This speleothem compilation is referred to here as the 5k compilation. Because not all speleothem $\delta^{18}O$ records cover the full 5 ka time window, it is separated into time slices of 1 ka duration, which overlap by 500 years. The overlapping allows us to join together the retrieved leading modes of the MC-PCA. Hence, in addition to the 5k compilation eight additional 1k compilations are analysed for their coherency. In total, nine different compilations of speleothem $\delta^{18}O$ records are analysed using MC-PCA, which are listed in Table 2.

4 Isotope modelling analysis (ECHAM5-wiso)

In order to better constrain the forcing of precipitation $\delta^{18}O$ (which is the ultimate source of speleothem $\delta^{18}O$ values) and the spatio-temporal pattern, which depicts the loading

Table 1 This table lists all speleothem $\delta^{18}O$ records used in this study and provides information on their respective cave systems

Speleothem	Cave	Latitude (°N)	Longitude (°E)	Altitude (m)	Mean Cave air temperature (°C)	Growth stop (ka BP)	Growth begin (ka BP)	Dating technique	References
BU-4	Bunker Cave	51.37	7.67	184	10.8	−0.06	8.2	TIMS	Fohlmeister et al. (2012)
CC-3	Crag Cave	52.23	−9.44	60	10.4	−0.05	10.1	TIMS	McDermott et al. (1999, 2001)
CC-26	Corchia Cave	44.00	10.22	840	7.5	0.695	11.205	ICP-MS	Zanchetta et al. (2007)
FM-3	Okshala Cave	67.00	15.00	200	3.2	−0.05	7.5	TIMS	Linge et al. (2009)
GAR-01	La Garma Cave	43.43	−3.66	75	12.1	−0.03	13.9	TIMS ICP-MS	Baldini et al. (2015)
J-1	Jeita Cave	33.95	35.65	100	22	1.2	12.2	ICP-MS	Cheng et al. (2015)
K-1	Korallgrottan	64.88	14.15	570	2.7	−0.06	3.8	TIMS	Sundqvist et al. (2010)
MB-3	Milchbach Cave	46.37	8.05	1840	2.5	2.2	9.2	ICP-MS	Luetscher et al. (2011)
SO-1	Sofular Cave	41.42	31.93	442	12	−0.06	50.3	ICP-MS	Fleitmann et al. (2009), Göktürk et al. (2011)
SPA-12	Spannagel Cave	47.12	11.67	2531	1.8	0.02	4.8	TIMS	Mangini et al. (2005)
SU-967	Uamh an Tartair	58.15	−4.98	220	7.2	−0.05	0.95	Lamina counting	Baker et al. (2011)

(i.e. coupling) of each speleothem $\delta^{18}O$ dataset with the respective PC, the precipitation $\delta^{18}O$ dataset of an isotope enabled General Circulation Model, ECHAM5-wiso (Langebroek et al. 2011; Werner et al. 2011), is also analysed for the period 1960–2012 AD for coherent pattern of the dominant mode using Principal Component Analysis (PCA). The analysed ECHAM5-wiso model output covers the sector from 40°W to 40°E and from 20°N to 80°N with a spatial resolution of 1.9° × 1.9°. (For details on the ECHAM5-wiso model see Werner et al. 2011 and Langebroek et al. 2011.) Although, the time period of the model simulation, being annual and covering only 42 years, is quite different to that of the analysed speleothem $\delta^{18}O$ records, having a temporal resolution of 30 years and covering at least 1 ka, the PCA analysis of the simulated precipitation $\delta^{18}O$ data of the ECHAM5-wiso model provide a first order benchmark of what could be expected in terms of the strength of the dominant mode and the mechanisms behind it, as well as the shape of the spatio-temporal pattern revealed by the loadings. Hence, we assume for the data-model comparison that the mechanism(s) that drive the precipitation $\delta^{18}O$ variability of the ECHAM5-wiso model are the same as for the past variability of speleothem $\delta^{18}O$ records.

European speleothems imprint mainly the precipitation weighted $\delta^{18}O$ signal of the winter precipitation that is infiltrated into the karst system and reaches the caves as cave drip water. For this reason we analysed the precipitation-weighted $\delta^{18}O$ signal ($\delta^{18}O_{pw}$) of the ECHAM5-wiso model in the sector from 40°W to 40°E and from 20°N to 80°N for the 4-month winter period (December–March) and an extended 6-month winter period from October to March (Fig. 3). The 4-month winter period is analysed to explore the effect of the North Atlantic Oscillation on $\delta^{18}O_{pw}$, which is strongest during this period; the 6-month winter period is analysed, because it reflects the main infiltration period in Europe and, therefore, the signal that is potentially recorded by speleothems. Furthermore, we have conducted an additional PCA analysis of selected grid cells in which the investigated cave systems are located (Fig. 4). The two leading modes of the 4- and 6-month winter period were then compared with the dominant winter mode of atmospheric circulation in this sector, the North Atlantic Oscillation (NAO) (Hurrell 1995). The winter NAO index (wNAOi) is calculated as described by Langebroek et al. (2011) for the period from December to March and is based on the sea level pressure field of the ECHAM5-wiso model in the sector from 40°W to 40°E and from 20°N to 80°N using PCA.

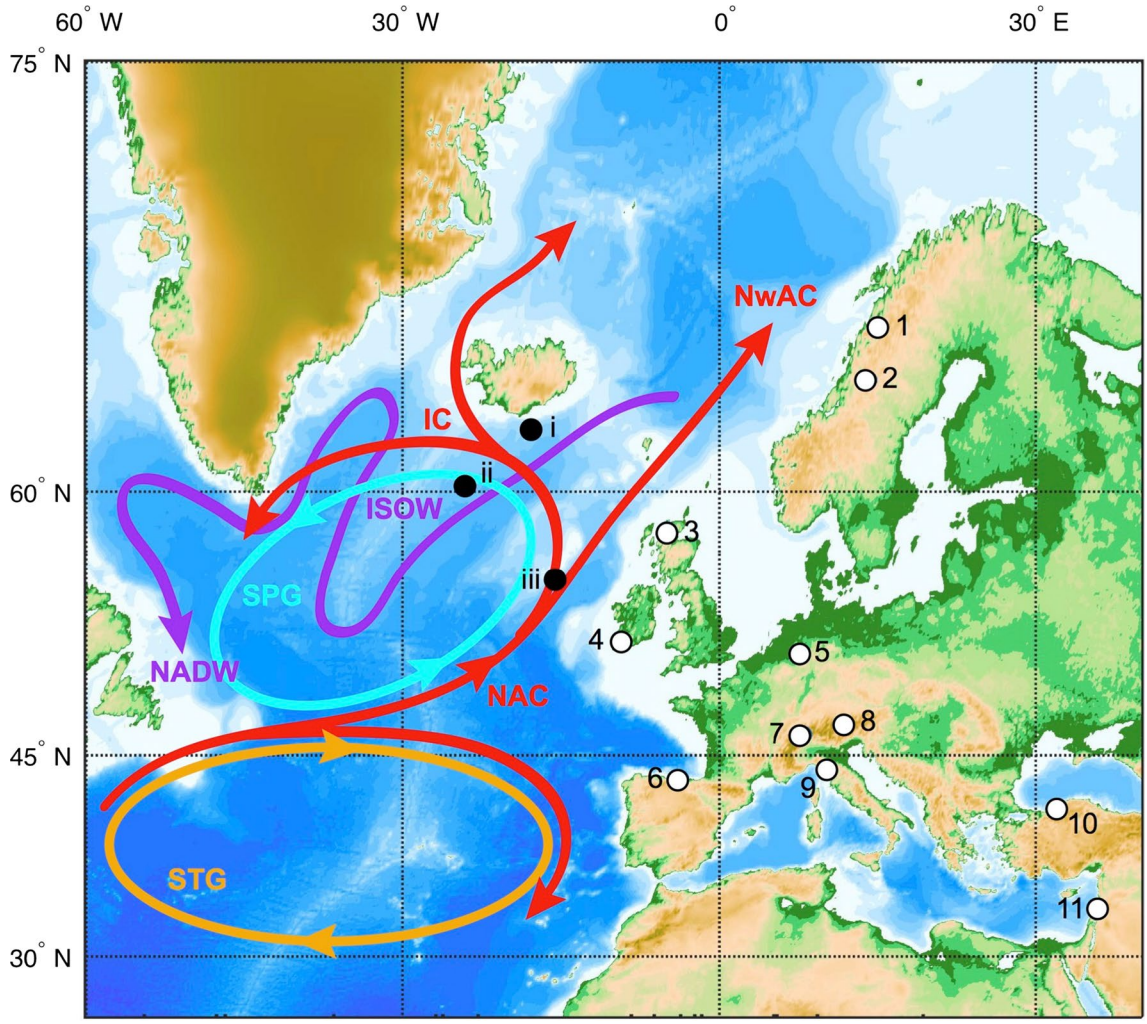

Fig. 2 Map illustrating the spatial distribution of used speleothem records: open circles depict the location of cave systems from which speleothem $\delta^{18}O$ records are used: (*1*) FM-3, Okshala Cave, Norway; (*2*) K-1, Korallgrottan, Sweden; (*3*) SU-69-7, Uamh an Tartair, Scotland; (*4*) CC-3, Crag Cave, Ireland; (*5*) BU-4, Bunker Cave, Germany; (*6*) GAR-01, La Garma Cave, Spain; (*7*) MB-3, Milchbach Cave, Switzerland; (*8*) SPA-12, Spannagel Cave, Austria; (*9*) CC-26, Corchia Cave, Italy; (*10*) SO-1, Sofular Cave, Turkey; (*11*) J-1, Jeita Cave, Lebanon. Detailed information on the cave systems and individual speleothems is given in Table 1. *Closed circles* indicate the position of cited sedimentary archives from the North Atlantic: (*i*) RAPiD-12-1k (Thornalley et al. 2009); (*ii*), GS06-144 08GC (Mjell et al. 2015); (*iii*) Various cores from "The Rockall Trough" (Copard et al. 2012). Furthermore, the *map* shows North Atlantic currents that are mentioned in this study: the *red* (*violet*) *colour* indicates surface (*bottom*) currents. *NAC* North Atlantic Current, *NwAC* Norwegian Atlantic Current, *IC* Irminger Current, *ISOW* Iceland Scotland Overflow Water, *NADW* North Atlantic Deep Water (note that the NADW is not only composed of ISOW but also of Denmark Straight Overflow Water, DSOW, and Labrador Sea Water, LSW). The *cyan* (*orange*) *coloured ellipse* indicates that approximate position of the subpolar (subtropical) gyre. *Arrows* indicate the flow direction. Note that not all features of the North Atlantic Ocean circulation are shown for simplicity

For the 4-month (December–March) analysis, the spatio-temporal pattern of the loadings of the 1st PC depicts a dipole-like pattern with positive loadings at the western margin and Central Europe and negative loadings over Iceland and East Greenland (Fig. 3a). The pattern is similar with the correlation map between the winter NAO index and winter $\delta^{18}O_{pw}$ values calculated by Langebroek et al. (2011) using also ECHAM5-wiso simulations. The NAO forcing of this pattern is further confirmed by the correlation between the 1st PC and the wNAOi ($r_s = 0.61$, $p < 0.01$) (Fig. 3b). The spatio-temporal pattern of the loading of the 2nd PC of the 4-month analysis reveals strong positive loadings over the Norwegian Sea. No clear pattern is observed over Central Europe. Furthermore, no correlation is observed between the 2nd PC and the wNAOi suggesting that this mode is characteristic for the Norwegian Sea and adjacent regions only (Fig. 3a, b).

The spatio-temporal pattern of the loadings of the 1st PC for the 6-month winter period (October–March) depict a dipole-like pattern that is similar to that observed for

Table 2 This table lists the compilations of speleothem $\delta^{18}O$ records investigated for spatio-temporal coherency using MC-PCA

Compilation	Period from (ka BP)	Period to (ka BP)	1st PC	Spatio-temporal coherency pattern	TEV of 1st PC (%)	Used speleothems (# number of speleothems)
5 ka	0.1	5	Figure 5a	Figure 6	24.51 ± 0.98	BU-4, CC-3, FM-3, GAR-01, SO-1, SPA-12 (#6)
1k.I	3.5	4.5	Figure 5b	Figure 7a	28.97 ± 2.03	BU-4, CC-3, CC-26, FM-3, GAR-01, J-1, MB-3, SO-1, SPA-12 (#9)
1k.II	3.0	4.0	Figure 5b	Figure 7b	25.48 ± 1.81	BU-4, CC-3, CC-26, FM-3, GAR-01, J-1, MB-3, SO-1, SPA-12 (#9)
1k.III	2.5	3.5	Figure 5b	Figure 7c	29.40 ± 2.35	BU-4, CC-3, CC-26, FM-3, GAR-01, J-1, K-1, SO-1, SPA-12 (#9)
1k.IV	2.0	3.0	Figure 5b	Figure 7d	26.76 ± 1.74	BU-4, CC-3, CC-26, FM-3, GAR-01, J-1, K-1, SO-1, SPA-12 (#9)
1 k.V	1.5	2.5	Figure 5b	Figure 8a	30.39 ± 2.06	BU-4, CC-3, CC-26, FM-3, GAR-01, J-1, K-1, SO-1, SPA-12 (#9)
1k.VI	1.0	2.0	Figure 5b	Figure 8b	32.29 ± 2.37	BU-4, CC-3, CC-26, FM-3, GAR-01, K-1, SO-1, SPA-12 (#8)
1k.VII	0.5	1.5	Figure 5b	Figure 8c	39.36 ± 3.53	BU-4, CC-3, FM-3, K-1, SO-1, SPA-12 (#6)
1k.VIII	0.01	1	Figure 5b	Figure 8d	43.84 ± 2.64	BU-4, CC-3, GAR-01, K-1, SO-1, SPA-12, SU-967 (#7)

The time interval, total variance (TEV) explained by the 1st PC and included speleothem $\delta^{18}O$ records are shown for each compilation

the 4-month winter period. The dipole-like pattern of the loadings for the 2nd PC pictures negative values over Central Europe and positive loadings over the Norwegian Sea (Fig. 3c). The correlation of both PCs with the wNAOi (1st PC: $r_s = 0.4$, $p < 0.01$; 2nd PC: $r_s = -0.46$, $p < 0.01$) suggests that the North Atlantic Oscillation is the dominant mode for the observed spatio-temporal patterns. Note that the correlation between the 2nd PC and the wNAOi is negative. Therefore, if the 2nd PC is flipped (which would result then in a positive correlation of the 2nd PC to the wNAOi), the spatio-temporal pattern is suggesting negative loadings over Scandinavia and the Norwegian sea and positive loadings over Central Europe.

The 6-month spatio-temporal pattern for the 1st and 2nd PC of the $\delta^{18}O_{pw}$ values at the investigated cave locations reveal that the central European cave locations lie within a zone where the 1st and 2nd PC show a positive relationship to the wNAOi. The $\delta^{18}O_{pw}$ values at the two Scandinavian cave sites are only little influenced by the 1st PC, but show a stronger dependence on the 2nd PC, suggesting a negative correlation to the wNAOi. The two cave sites in northern Turkey and the northern Levant do exhibit a weak influence of the wNAOi on $\delta^{18}O_{pw}$ values (Fig. 3). To better constrain the spatio-temporal pattern that is retrieved from the investigated speleothem $\delta^{18}O$ time-series records, we investigate a reduced dataset of $\delta^{18}O_{pw}$ values. For this only the 6-month $\delta^{18}O_{pw}$ data from grid cells were used where the investigated caves sites are located (Fig. 4).

The spatio-temporal pattern derived from the PCA analysis of this reduced dataset provides an additional tool to interpret and assess spatio-temporal patterns derived from MC-PCA analysis of speleothem $\delta^{18}O$ compilations (see Sect. 6.3). The results of this analysis indicate that the $\delta^{18}O_{pw}$ values in central Europe have a strong positive loading to the 1st PC, while the $\delta^{18}O_{pw}$ values for the two sites in Scandinavia have a weak negative loading to the 1st PC. The two sites in northern Turkey and the northern Levant have a weak positive loading to the 1st PC (Fig. 4). This computed pattern of selected grid cells is in accordance with the observed spatio-temporal pattern found for all grid cells for the 6-month winter period (Fig. 3c). The 1st PC of the reduced dataset is significantly correlated to the wNAOi ($r_s = 0.42$, $p < 0.01$) suggesting that the NAO is the dominant mode that controls first order changes in $\delta^{18}O_{pw}$ values at the cave locations. Note that, although the NAO is the dominant mode of $\delta^{18}O_{pw}$ variability of the selected grid cells, it explains only about 27.6 % of its total variance. This is a rough benchmark for the total explained variance

that would be expected from MC-PCA analysis of speleothem $\delta^{18}O$ records whose ultimate source is $\delta^{18}O_{pw}$.

5 Results

5.1 Principal components

Rule KS2 indicates that the 1st PCs of all investigated compilations (Table 2) are potentially meaningful at a 95 % confidence level (Table 3 and Fig. 1, Figures S6–S8). Furthermore, a comparison with the white noise null model of Rule N shows that all 1st PCs of every analysed compilation, except compilation 1k.II, is above the 95 % confidence level. However, the red noise null model of Rule N shows that only the 1st PC of compilation 1k.VIII is above the 95 % confidence level. For all other compilations the red noise model was not rejected, which suggests that the speleothems contain no common signal beyond red noise. The 1st PC, however, may be particularly dominant over the last 1000 years. Taking account of the results of these selection rules, the 1st PCs of all 1k compilations and their respective spatio-temporal patterns are considered further in this study for comparisons with other palaeoclimate records (Sect. 6.2).

The mean 1st PCs of the 5k and the 1k compilations are illustrated in Fig. 5a, b, respectively. It is noteworthy, that the comparison of the eight 1st PCs of the 1k compilations reveals that the mean 1st PCs and the respective 1-sigma uncertainties are similar in the overlapping periods. The good agreement between the individual 1st PCs of the 1k compilations suggests that they reflect the same large-scale speleothem $\delta^{18}O$ modulating signal. Therefore, we discuss this record as a whole and not each 1st PC individually. In the following, we label the 1st PC of compilation 5k (reflecting a common mode of speleothem $\delta^{18}O$ variability) as the *common speleothem record 5k* (CSR5k) and the aligned 1st PC records of all 1k compilations as CSR1k record.

The CSR5k record shows that the values of the record are smaller between 5 and 4 ka BP in comparison to the values of the last 4 ka. Values increase gradually until about 4 ka BP and reached a constant average value during the last 4 ka. In this period, a quasi-periodic variability is observed. The CSR5k record shows a sharp minimum at about 3.5 ka BP, and other minima at approximately 2.2 ka BP and from about 1.2 to 0.76 ka BP. Compared with the second and third minima, the first minima at c. 3.5 ka BP is a short event, whereas the second and third minima last for about 250 and 500 years, respectively. Between 4 and 0.1 ka BP, the CSR5k record shows three major maxima, the first of which lasts for about 500 years and ranges from 3.25 to 2.75 ka BP with a plateau-like shape, though there are changes of higher frequency during this time (including the sharp minima). The second maximum is more distinct than the first, and reaches the highest value between 1.75 and 1.5 ka BP. A third maximum is observed at about 0.5 ka BP. The high value of the second maximum is caused by speleothem SO-1 (verified by an additional MC-PCA; not shown here) that has a maximum at about the same time (Figure S4).

The CSR1k record (Fig. 5b) shows a quasi-periodic cyclicity during the last 4.5 ka. The record shows maxima centred at around 4, 2.75, 1.75 and 0.5 ka BP, and minima centred on c. 3.5, 2 and 0.9 ka BP. From about 0.01 to 0.2 ka BP the values of the CSR1k record are similar to the minima. Although the appearance of the minima and maxima appears to be quasi-periodic, the course of each extremum is different. The first two maxima (centred on 4 ka BP and 2.75 ka) last longer compared with the others (centred on 1.75 ka BP and 0.5 ka). The very positive value of the second maxima from 1 ka.V is caused by speleothem SO-1, as it is the case for the CSR5k record (not shown here). Interestingly, the shape of the last maximum (at 0.5 ka BP) coincides with the Little Ice Age development from 0.76 to 0.1 ka BP (Lamb 2002) and its development is more rapid compared to all other maxima. The minima are comparable in duration, although the beginning of the last minimum, that coincides with the Medieval Climate Anomaly (MCA) (Lamb 2002), is reached by an intermediate state centred at about 1.25 ka BP (Fig. 5b).

Comparison of the CSR5k and CSR1k records shows that they differ in the period from 4.5 to 3 ka BP (Fig. 5). The sharp minimum of the CSR5k record at about 3.5 ka BP occurs at the same time as the minimum in the CSR1k record, but the shape of both maxima is clearly not comparable. In the time between 2.5 and 0.1 ka BP the two records look similar, although there are differences of higher order. These differences are also confirmed by FFT analysis and a cross-wavelet transform (Grinsted et al. 2004) on the mean CSR1k and CSR5k records (Figure S10). This analysis reveal that the two records are alike for low-frequency signals (c. 1000–1500 years periodicity) in the period from 3.5 to 0.0 ka BP whereas there are no shared periodicities in the time between 4.5 and 3.5 ka BP. (The cone of influence may distort the significance tests of the cross-wavelet transform at the boundaries, see Figure S10.) The differences between the two records, in particular in the period from 4.5 to 3.5 ka BP can be caused by the different compilations of speleothem $\delta^{18}O$ records: for the CSR5k compilation only six speleothem $\delta^{18}O$ records are used, whereas nine records are used for compilations 1k.I to 1k.III. However, this is rejected by an additional MC-PCA analysis of the CSR5k compilation using, as for the CSR1k compilations, 1 ka-long time slices. The results for the 1st PC of this exercise show a variability that is akin to that of the CSR1k record (Figure

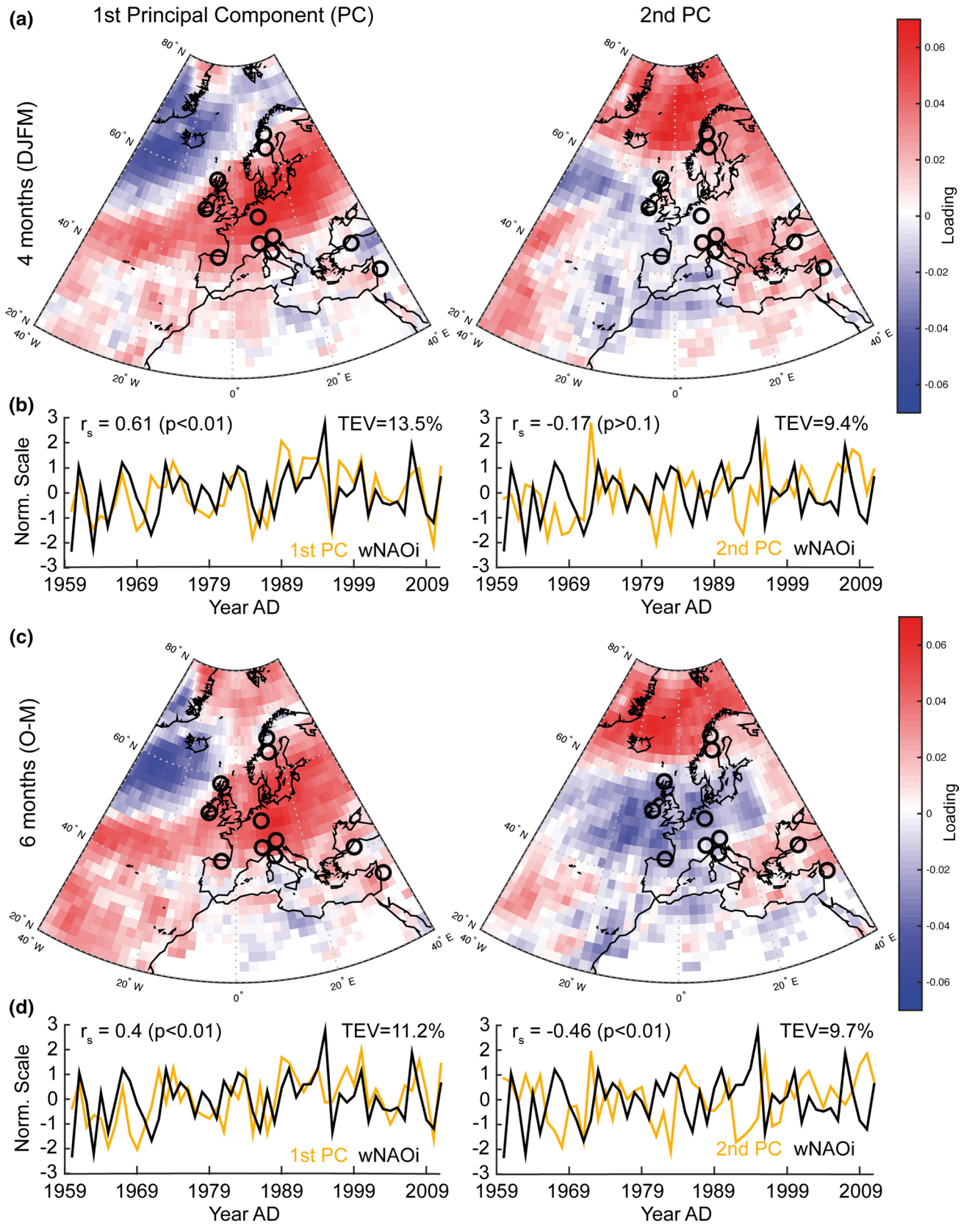
(a)
1st Principal Component (PC)
2nd PC
4 months (DJFM)
Loading
(b)
r_s = 0.61 (p<0.01)
TEV=13.5%
r_s = -0.17 (p>0.1)
TEV=9.4%
Norm. Scale
1st PC wNAOi
2nd PC wNAOi
Year AD
(c)
6 months (O-M)
(d)
r_s = 0.4 (p<0.01)
TEV=11.2%
r_s = -0.46 (p<0.01)
TEV=9.7%

◂**Fig. 3** The maps and figures illustrate the results of the PCA conducted on boreal winter (4 months, from December to March; 6 months from October to March) ECHAM5wiso (T63L31) precipitation-weighted precipitation $\delta^{18}O$ time series ($\delta^{18}O_{pw}$) in the period from 1960–2012 AD in the sector from −40 to 40°E and from 20 to 80°N. The maps depict the spatio-temporal pattern of the loading between the 1st and 2nd PC and $\delta^{18}O_{pw}$ time series of each grid cell; the figures show the temporal history of the 1st and 2nd PC and the winter NAO index (wNAOi). **a** Illustrate the spatial pattern of the loading of the 1st (*left*) and 2nd (*right*) PC for the 4-months winter period. The *colour bar* on the *right hand side* indicates the colour code for the loadings for both maps; in general positive (negative) values are indicated in *red* (*blue*). The *black circles* indicate the location of the speleothems investigated in this study. **b** The figures for the time history of the 1st (*left*) and 2nd (*right*) PC (*orange*) and the wNAOi (*black*). Furthermore, the Spearman's rank correlation coefficient (r_s) (and its *p* value) and the total explained variance (TEV) of the respective PCs are shown. The 2nd PC shows no correlation with the wNAOi, whereas the 1st PC is clearly correlated to the wNAOi. **c**, **d** The same maps and figures as for (**a**) and (**b**) but for the 6-month winter period $\delta^{18}O_{pw}$ time series. Both PCs show a significant correlation to the wNAOi

S11). We attribute the different results of the average 1st PC to the length of the time slices. For the entire 5 ka-long time slice the PCA weighted the stalagmite records the most that have the highest absolute variability in $\delta^{18}O$. If the variance is, however, not stationary in time (perhaps due to changing isotope disequilibrium effects that can act to amplify or attenuate the variability), the PCA might miss variability in other records. This is evident for example for stalagmite BU-4 that has a high variability in the period from 1.0 to 0.0 ka BP but low variability in the period between 5.0 and 1.0 ka BP (Figure S4). We therefore conclude that the 1 ka-long time slices are better to constrain the spatio-temporal variability of all palaeoclimate proxy records. For this reason, comparisons with other palaeoclimate records focuses hereafter on the CSR1k record, which is considered to best capture the dominant mode of speleothem $\delta^{18}O$ variability.

5.2 Spatio-temporal coherency pattern

The spatio-temporal pattern for each of the nine compilations is shown in Figs. 6, 7 and 8. The median loading for each speleothem and for each compilation and its standard deviation is listed in Table 4. A positive (negative) loading denotes that a speleothem's $\delta^{18}O$ values increase (decreases) if the 1st PC increases.

The spatio-temporal pattern for the 1st PC of the 5k compilation (Fig. 6) illustrates the mean state of the loading for the period from 0.1 to 5 ka BP between the 1st PC and each individual speleothem $\delta^{18}O$ record. It illustrates strong positive loadings in Central Europe (BU-4, Germany; SPA-12, Austria) and in Northern Turkey (SO-1, Turkey). Negative loadings are observed for speleothem $\delta^{18}O$ records at the western margin of Europe (CC-3, Ireland; GAR-01, Spain) and northern Scandinavia (FM-3, Norway).

The spatio-temporal patterns for the 1st PC for each of the 1k compilations are illustrated in Figs. 7 and 8. For the time slices covering the period from 4.5 to 2 ka BP (compilation 1k.I–1k.IV) (Fig. 7), the spatio-temporal pattern presents a persistent pattern of positive loadings in the Alps (MB-3, Switzerland; SPA-12, Austria) and negative loadings for BU-4 (Germany) and northern Italy (CC-26). The loading for SO-1 (northern Turkey) is negative for the two time slices from 4.5 to 3.5 ka BP (1k.I) and from 4.0 to 3.0 ka BP (1k.II) but changes to positive values for the time slices from 3.5 to 2.5 ka BP (1k.III) and from 3.0 to 2.0 ka BP (1k.IV). The loading for J-1 (northern Levant) show high positive loadings for the 4.5 to 2.5 ka BP (1k.I–1k.III) time slice, changing to a negative loading for the 3.0 to 2.0 ka BP time slice (1k.IV). Similar changes are observed for the other cave locations, in particular the sign of the loading for CC-3 (Ireland) and GAR-01 (Spain) changes for every time slice. The spatio-temporal pattern for the time slices from 2.5 to 0.01 ka BP (compilation 1k.V–1k.VIII) (Fig. 8) is more continuous through this entire period compared to the 1k time slices of the period of identical duration from 4.5 to 2.0 ka BP (Fig. 7a–d). Note that the spatio-temporal pattern is also similar for the two successive time slices from 3.0 to 2.0 ka BP (Fig. 7d) and from 2.5 to 1.5 ka BP (Fig. 8a). For the period from 2.5 to 1.5 ka BP (compilation 1k.V), positive loadings are observed for the speleothem $\delta^{18}O$ records in the Alps (SPA-12, Austria) and northern Turkey (SO-1), while all other loadings are negative. The highest loadings are observed for CC-3 (Ireland), FM-3 (Norway), BU-4 (Germany) and J-1 (Lebanon) (Fig. 8a). Compared with the previous time slice, the sign of the loadings changes in central Europe (BU-4, Germany), northern Italy (CC-26) and northern Scandinavia (K-1, Sweden; FM-3, Norway) from negative to positive values for the 2 to 1 ka BP time slice. The sign of all other loadings is unchanged (Fig. 8b). For the time slice from 1.5 to 0.5 ka BP, only the sign of the loading of SO-1 changes from positive to negative (Fig. 8c); the spatio-temporal pattern for the time slice from 1 to 0.01 ka BP is unchanged compared with the previous diagram (Fig. 8d).

A discussion of the observed spatio-temporal pattern and the comparison with the spatio-temporal pattern derived for the ECHAM5-wiso simulations follows in the next section after the physical meaning of the CSR records is discussed.

6 Discussion

6.1 Causes for coherency of speleothem $\delta^{18}O$ values

Our results reveal that European speleothem $\delta^{18}O$ datasets exhibit strong large-scale spatio-temporal coherency during the last 5 and 4.5 ka, expressed by the CSR5k and CSR1k records (CSR records), respectively. Interpreting

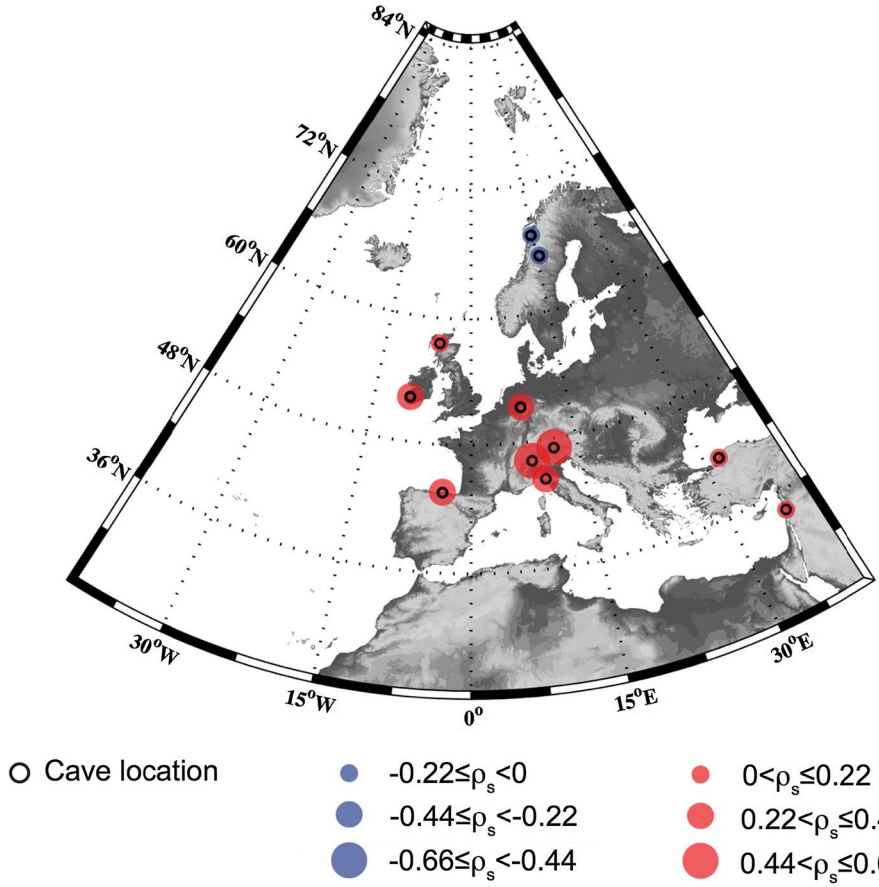

Fig. 4 This map illustrates the spatio-temporal pattern of the loading (ρ_s) between the 1st PC and ECHAM5wiso (T63L31) winter (October–March) precipitation-weighted precipitation $\delta^{18}O$, using only the time series of grid cells containing the caves of the investigated stalagmites. The time series of each grid cell was normalised prior to the PCA procedure to ensure that all grid cells have a similar variance. The 1st PC explains about 27.6 % of the total variance of the selected grid cells (the 2nd PC about 20.1 %). The Spearman's rank correlation coefficient between the 1st PC and the wNAOi is 0.42 ($p < 0.01$). Positive (negative) loadings are indicated as *red* (*blue*) circles at the location of the speleothem records; the size of a *circle* denotes the strength of the loading. The *open black circles* show the locations of the caves from which the speleothems were collected

Table 3 This table lists the selected PCs for every compilation that are "potentially meaningful" for each selection rule

	5k	1k.I	1k.II	1k.III	1k.IV	1k.V	1k.VI	1k.VII	1k.VIII
Rule KS2	1–6	1–2	1–2	1–2	1	1–3	1, 3	1–2	1–4
Rule N (WN)	1	1	–	1	1	1	1	1	1–2
Rule N (AR1)	–	–	–	–	–	–	–	–	1
Selected PC	1	1	1	1	1	1	1	1	1

1st row Rule KS2 (95 % confidence); 2nd row Rule N, white noise null model (95 % confidence); 3rd row Rule N, red noise null model (95 % confidence); See Sect. 2.3 for details on the respective selection rules and Fig. 1, Figure S6, Figure S7 and Figure S8 for the test of the respective null models on the PCs. The selected PC (last row) is the most dominant PC (highest eigenvalue) found to be "potentially meaningful" by Rule KS2

the physical meaning of the CSR records requires consideration of both the local and regional-scale processes that could have influenced speleothem $\delta^{18}O$ values (e.g. Jex et al. 2013; Lachniet 2009; McDermott 2004). These processes need to be distinguished in terms of processes that imprint a large-scale coherent climate-related signal in the speleothem $\delta^{18}O$ records versus local site-specific processes that may contribute to "noise" and therefore degrade the large-scale coherent signals. The large-scale coherent signals could be forced by a common mode such as

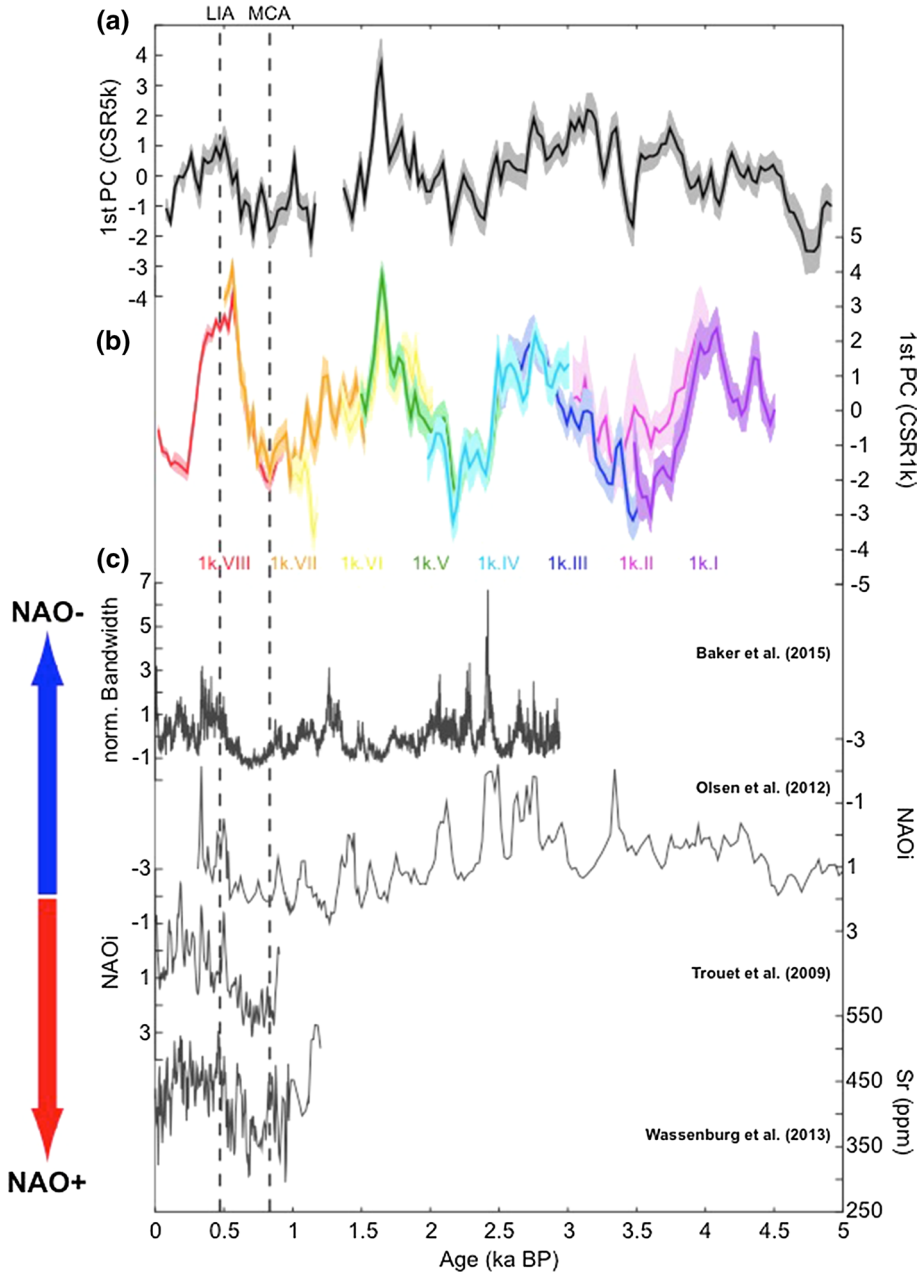

Fig. 5 **a** Illustrates the 1st PCs of the 5 ka compilation (CSR5k) containing the speleothem $\delta^{18}O$ records of FM-3, CC-3, BU-4, GAR-01, SPA-12 and SO-1. The *black line* is the mean value of the 1st PC, calculated from 2000 Monte Carlo simulations. The *grey shaded area* indicates its 1-sigma standard deviation. **b** The mean 1st PCs of the 1 ka compilations (CSR1k) from compilation 1k.I though to 1k.VIII (older to younger). The *shaded area* indicates the 1-sigma standard deviations. The mean values as well as the standard deviations are calculated from the results of 2000 MC simulations conducted for every speleothem compilation. The standard deviations expresses the uncertainty of the mean 1st PC caused by variable temporal resolutions and age uncertainties of individual speleothem time series. **c** Various reconstruction of the NAO index. These reconstructions indicate a persistent positive NAO index during the MCA and a primarily negative NAO index during the LIA. Hence, more positive (negative) values of the CSR records are associated with a negative mode of the NAO, indicating southward (northward) shifted westerlies. LIA indicates the Little Ice Age development and MCA the Medieval Climate Anomaly

the North Atlantic Oscillation that affects winter temperature and precipitation pattern (e.g. Hurrell 1995). Another aspect that has more recently come into focus is the relationship of the NAO to European precipitation $\delta^{18}O$ values and atmospheric teleconnection patterns (Baldini et al. 2008; Field 2010; Langebroek et al. 2011; Mischel et al. 2015). Furthermore, the geographic pattern of NAO-related effects on temperature, precipitation and precipitation $\delta^{18}O$ can be modified in some parts of Europe by concomitant variations in the East Atlantic (EA) pattern (Comas-Bru and McDermott 2013; Comas-Bru et al. 2016). Overall, persistent changes of the winter mode of the NAO (frequency of NAO+ vs. NAO−) can be a reasonable forcing mechanism to interpret the physical meaning of the CSR records. This conclusion is supported by Langebroek et al. (2011) and by the PCA analysis of ECHAM5-wiso simulations conducted in this study identifying the NAO as the major mode of variability for $\delta^{18}O_{pw}$ during the European winter period.

In principle, local-scale processes can also modify the $\delta^{18}O$ signal recorded by speleothems. However, these processes typically operate at a local, site-specific scale, and are thought unlikely to act in concert to produce the observed first-order coherent spatio-temporal evolution of the CSR records on a large-scale. However, isotope disequilibrium effects (Deininger et al. 2012; Mühlinghaus

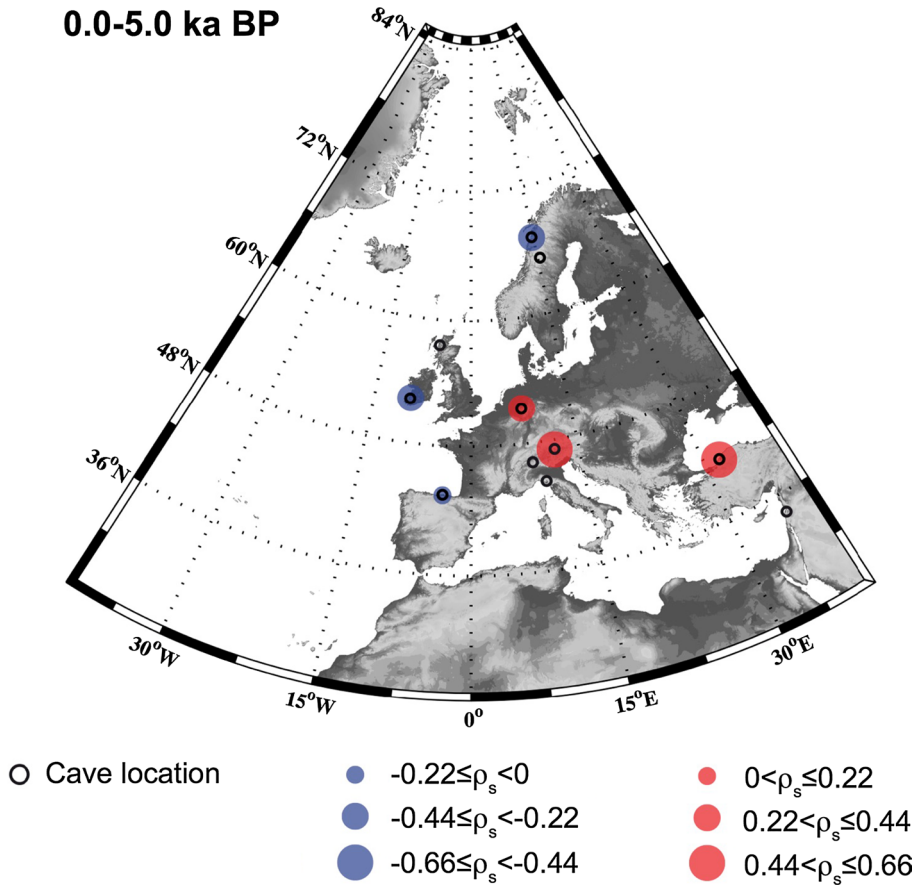

Fig. 6 This map illustrates the spatio-temporal pattern of the loading (ρ_s) between the 1st PC and speleothem $\delta^{18}O$ records. The loadings convey the strength of the coupling to the 1st PC for the speleothem $\delta^{18}O$ records that span the last 5 ka continuously. The *open black circles* show the location of the cave systems from which the speleothems were originally collected. The median of each loading between a speleothem's $\delta^{18}O$ record and the 1st PC is calculated from the ensemble of all loadings computed from 2000 Monte Carlo simulations. Positive (negative) medians are highlighted as *red* (*blue*) circles at the location of each speleothem record; the size of a *circle* denotes the strength of the loading. If a speleothem record is not used for a compilation only the location of the speleothem record is illustrated in the map. For this 5 ka compilation, speleothems FM-3, CC-3, BU-4, GAR-01, SO-1 and SPA-12 were used

et al. 2009) that depend on cave air temperature and drip interval could act in tandem with large-scale climate changes in temperature or precipitation to modify $\delta^{18}O$ during the formation of speleothems. Thus, while we cannot rule out a role for local site-specific processes that may have accentuated or dampened the speleothem $\delta^{18}O$ response to European-scale climate changes, we argue that the observed spatio-temporal coherency in speleothem $\delta^{18}O$ is likely driven by large-scale aspects of the climate system, possibly by a NAO-type forcing. To better constrain the physical meaning of the CSR records, they are compared with sedimentary records from the North Atlantic Ocean (Sect. 6.2). The derived spatio-temporal patterns are discussed in Sect. 6.3.

6.2 Discussion of the common speleothem records and there physical interpretation

In agreement with reconstructions of the winter NAO index, suggesting a negative (positive) NAO index during the LIA (MCA) (Baker et al. 2015; Trouet et al. 2009; Wassenburg et al. 2013), positive (negative) values of the CSR records are interpreted to reflect primarily NAO− (NAO+) modes, or southward and northward shifted westerlies, respectively (Fig. 5). The good agreement of the CSR records, in particular of the CSR1k record with sedimentary records from the North Atlantic Ocean supports this conclusion and is discussed in the following. The location of the sedimentary archives and features of the North Atlantic Ocean circulation mentioned in this study are shown in Fig. 2.

A recent reconstruction of the strength of the Iceland Scotland Overflow Water (ISOW) (Mjell et al. 2015) indicates that vigorous ISOW and related deep water formation in the Arctic Ocean coincide with minima in the CSR1k record (Fig. 9c). A recent modelling study (Yang et al. 2016) demonstrated that the Atlantic Meridional Overturning Circulation (AMOC), which the ISOW is a component, can be modulated by changes in the wind stress on the ocean surface, such that a reduced wind stress triggers a slowdown of the AMOC. Although the study focused mainly on global wind stress effects on the AMOC, the authors state that similar results are obtained if the wind stress is reduced only over the North Atlantic (Yang et al. 2016). Based on this result, we conclude that a reduction (increase) of the ISOW can be related to a reduced (enhanced) wind stress over the North Atlantic, linked to southward (northward) shifted westerlies, akin to modulation of the westerlies by a NAO-type forcing. This conclusion is consistent with Visbeck et al. (2003) who showed that for positive modes of the NAO, the wind stress on the

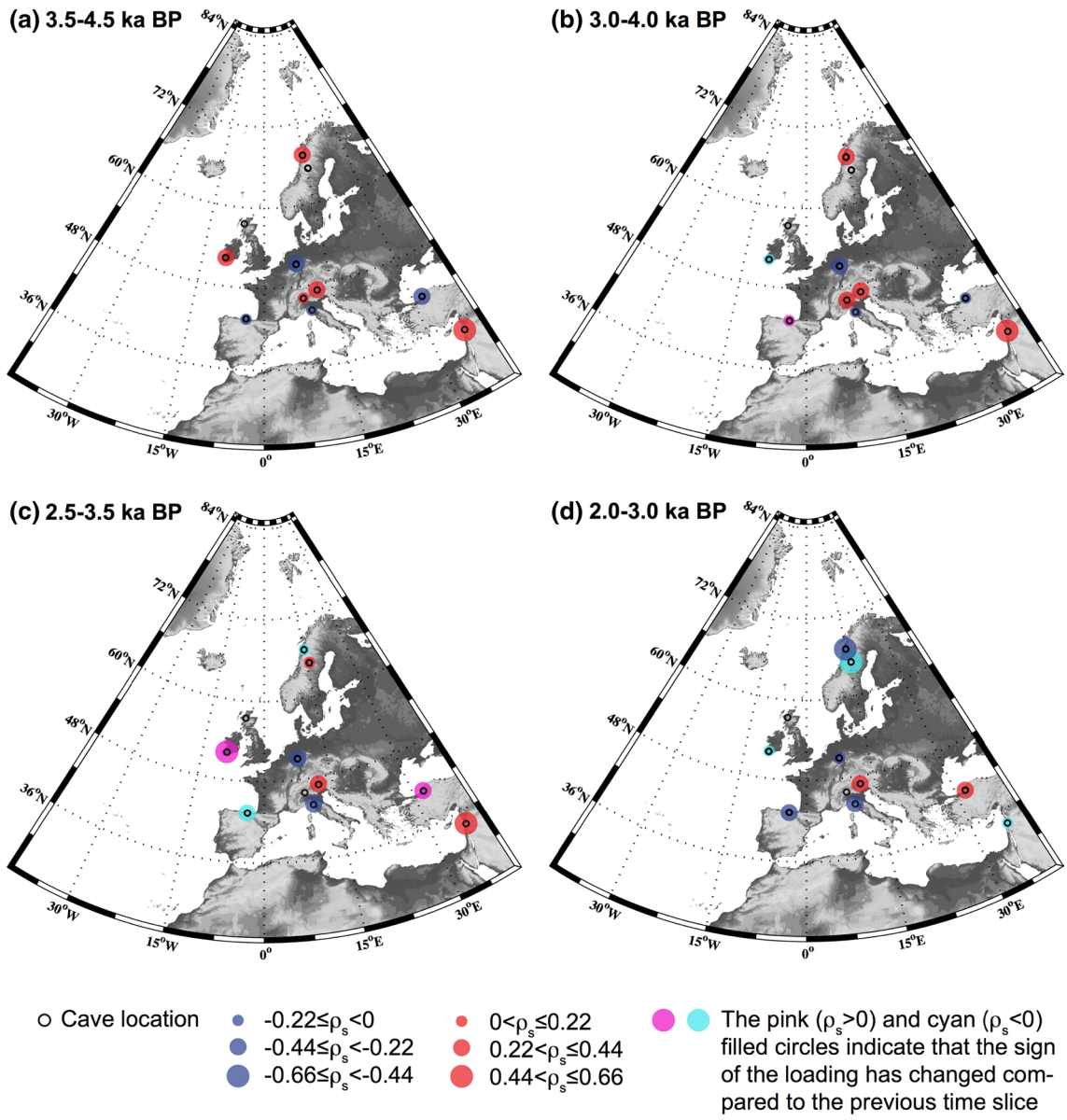

Fig. 7 Similar to Fig. 6, but for the 1k compilations (1 ka.I to 1 ka. IV). **a**–**d** The spatio-temporal pattern of the loading (ρ_s) for speleothem compilations 1 ka.I to 1 ka.IV (see Table 2 for details of each compilation). Locations where the sign of the median loading changed compared to the preceding time slice are highlighted: negative loadings are indicated in *cyan* (instead of *blue*) if the loading changed from positive to negative, and in *pink* (instead of *red*) if the loading changed from negative to positive

ocean increases in the sector of the subpolar gyre (SPG); interpreted as a meridional shift of the mean wind pattern (Marshall et al. 2001). Furthermore, this comparison shows that a higher flux of ice rafting debris (IRD) into North Atlantic sediments (Bond et al. 1997, 2001) (BO-0 to BO-3) occurred during what we infer to be predominantly southward shifted westerlies (negative NAO modes) during the last 5 ka (Fig. 9f), because of enhanced transport of sea ice (Blindheim and Østerhus 2005) and cooler sea surface temperatures during these periods of NAO− like conditions. This is further supported by the model simulations of Yang et al. (2016) demonstrating a southward sea ice expansion in the North Atlantic during reduced wind stress on the ocean—acting also as a positive feedback mechanism for a reduced AMOC.

The comparison of the CSR1k record with a reconstruction of the strength of the subpolar gyre (SPG) (Thornalley et al. 2009) indicates that periods of a stronger SPG roughly coincide with minima in the CSR1k record (Fig. 9b) (northward shifted westerlies), more vigorous ISOW (Fig. 9c) and a reduced southward sea ice expansion in the North Atlantic (Fig. 9f). The study of Thornalley

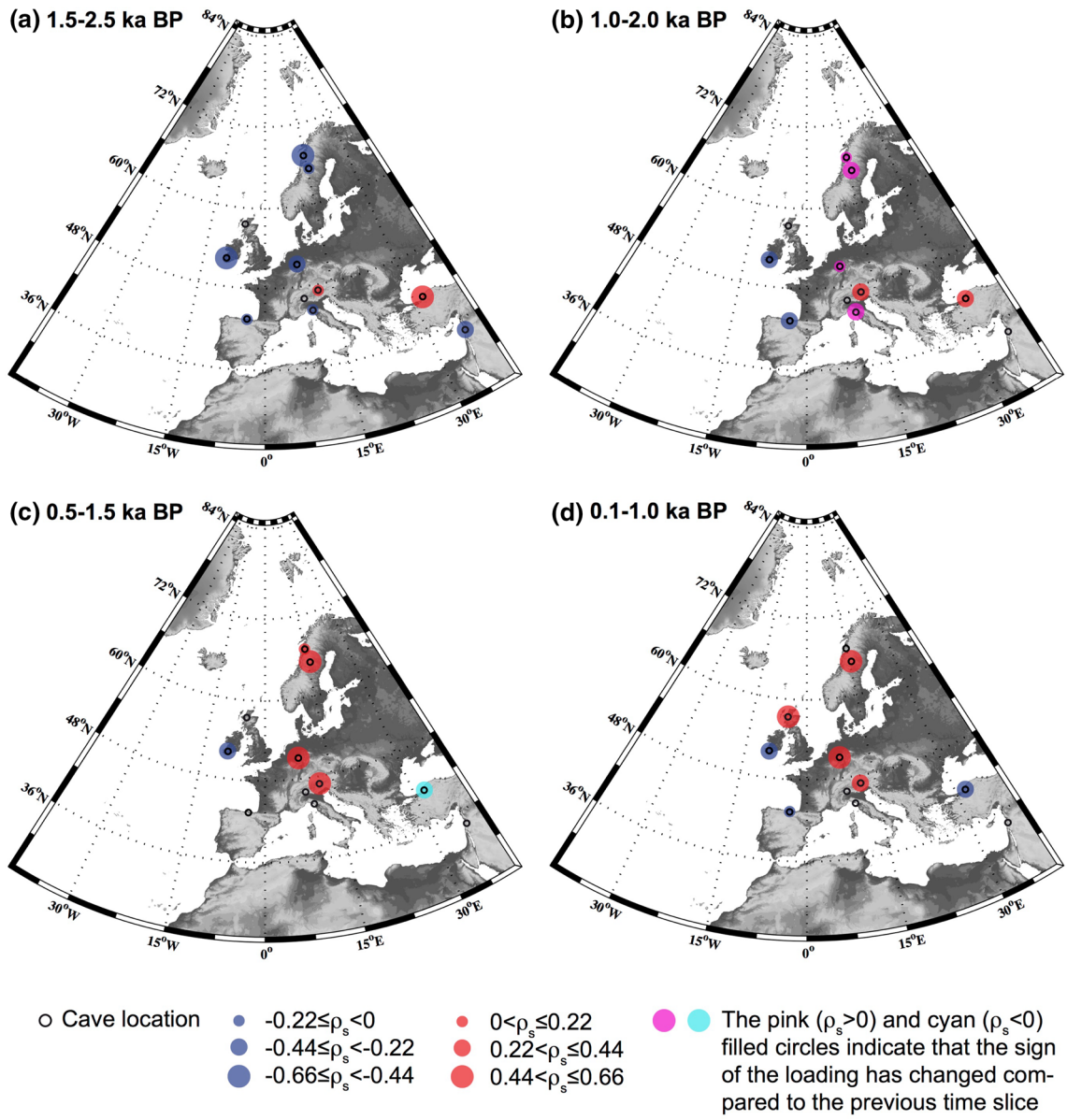

Fig. 8 Similar to Fig. 7, but for the 1k compilations V through to VIII. See Table 2 for details of the speleothems used in each compilation

et al. (2009) linked the strength of the subpolar gyre (SPG) to the upper-water-column density-difference ($\Delta\sigma$) that is modulated by the water source of the near-surface layer. If the density difference is small, more water is sourced from the cold, fresh SPG. By contrast, if the density difference is greater, the near-surface Atlantic water at this latitude is dominated by warm, saline subtropical gyre (STG) water (Thornalley et al. 2009). This concept is further supported by a comparison of the density-difference record with an independent record from the northeastern Atlantic (The Rockall Trough) based on the $^{143}Nd/^{144}Nd$ isotope ratio (expressed as εNd)—a conservative water mass tracer-recorded by deep-sea corals during the last 1.1 ka (Copard et al. 2012) (Figure S12). Thornalley et al. (2009) argued that changes of the wind stress on the ocean surface are responsible for the two-mode variability of the strength of the SPG during the last 5 ka. The strength of the SPG increases for an enhanced wind stress and decreases for a reduced wind stress. Hence, decreasing $\Delta\sigma$ implies a northward advance of westerlies, whereas increasing $\Delta\sigma$ suggests a southward advance of westerlies.

Compared to the mechanism proposed by Thornalley et al. (2009), our comparison reveals in detail that the minima and maxima of the strength of the SPG lag the extrema of the CSR1k record—and the reconstruction of sea ice expansion and ISOW history, respectively (Fig. 9).

Table 4 The table lists the median loadings of the first eigenvector (and their 1-sigma standard deviations) for the respective time period

	5k	1k.VIII	1k.VII	1k.VI	1k.V	1k.IV	1k.III	1k.II	1k.I
BU-4	0.39 (±0.12)	0.47 (±0.10)	0.50 (±0.12)	0.20 (±0.17)	−0.28 (±0.12)	−0.14 (±0.16)	−0.41 (±0.11)	−0.45 (±0.23)	−0.33 (±0.08)
CC-3	−0.39(±0.08)	−0.26 (±0.02)	−0.34 (±0.06)	−0.45 (±0.06)	−0.49 (±0.04)	−0.12 (±0.12)	0.48 (±0.04)	−0.06 (±0.19)	0.34 (±0.08)
CC-26				0.35 (±0.08)	−0.20 (±0.09)	−0.37 (±0.07)	−0.25 (±0.09)	−0.09 (±0.27)	−0.17 (±0.11)
FM-3	−0.35 (±0.07)		0.15 (±0.07)	0.09 (±0.1)	−0.46 (±0.04)	−0.44 (±0.05)	−0.19 (±0.07)	0.36 (±0.12)	0.43 (±0.05)
GAR-01	−0.21 (±0.09)	−0.17 (±0.03)		−0.37 (±0.08)	−0.20 (±0.06)	−0.25 (±0.07)	−0.29 (±0.06)	0.18 (±0.15)	−0.05 (±0.11)
J-1					−0.27 (±0.07)	−0.13 (±0.10)	0.46 (±0.04)	0.45 (±0.17)	0.51 (±0.04)
K-1		0.54 (±0.01)	0.51 (±0.04)	0.45 (±0.05)	−0.19 (±0.10)	−0.46 (±0.05)	0.10 (±0.08)		
MB-3								0.41 (±0.18)	0.15 (±0.07)
SO-1	0.55 (±0.07)	−0.36 (±0.02)	−0.29 (±0.06)	0.41 (±0.05)	0.47 (±0.04)	0.40 (±0.06)	0.30 (±0.06)	−0.12 (±0.29)	−0.41 (±0.08)
SPA-12	0.46 (±0.08)	0.27 (±0.03)	0.52 (±0.03)	0.30 (±0.05)	0.19 (±0.07)	0.38 (±0.06)	0.32 (±0.05)	0.23 (±0.27)	0.31 (±0.08)
SU-967		0.45 (±0.02)							

Empty fields denote that this speleothem was not included in the particular compilation

However, if the accumulated CSR1k record is compared to the Δσ reconstruction, it exhibits a much better temporal coherence to the Δσ reconstruction (Fig. 9b). (Accumulated CSR1k record means that the values of the CSR1k record are added together from oldest to youngest; see Figure S13 for detail.) A similar accumulated-NAO forcing has been recently identified to modulate the Atlantic Multidecadal Oscillation (AMO) in which ocean circulation acts as an intermediary (McCarthy et al. 2015). The comparison of the accumulated CSR1k record and the Δσ reconstruction indicates that the ocean circulation integrates the CSR1k forcing—or in other words ocean circulation integrates the wind stress forcing driven by the northward and southward shifted westerlies. Another modelling study has recently shown that large amounts of fresh water (i.e. melting sea ice) can trigger a shift of the SPG modes from strong to weak (Moreno-Chamarro et al. 2016) and we cannot exclude such effects here. However, the temporal shift between the minima and maxima of the ocean stacked IRD index (Bond et al. 1997, 2001) and the SPG reconstructions hints that this might be not the triggering mechanism. In summary, our comparisons between the marine sedimentary reconstructions support the hypothesis that more positive (negative) values of the CSR1k record indicate periods of primarily southward (northward) shifted westerlies—decreasing (increasing) the wind stress on the North Atlantic.

This conclusion is further supported by recent reconstructions of Holocene storm periods (HSP) from estuarine and coastal sedimentary records from northwestern France (Sorrel et al. 2012), and from the coastal dune fields of Jutland in Denmark (Clemmensen et al. 2009) demonstrating that HSP II, III, IV and partially V coincide with maxima of the CSR1k record (Fig. 9a). These HSPs are associated with a southward advance of the westerlies and associated storm tracks and resemble NAO− like modes of atmospheric circulation (Sorrel et al. 2012; Clemmensen et al. 2009). Therefore, two independent records for Δσ and HSP indicate that during the last 5 ka quasi-periodic changes between persistent northward and southward advances of the westerlies occurred, resembling a northward advance and a southward advance of the westerlies. Comparison of the CSR records with these episodic changes of North Atlantic Ocean surface hydrology show that increasing values of the CSR1k record are in phase with conditions of southward advancing westerlies while decreasing values coincidence with conditions of a northward migration of the westerlies. Hence, these oceanic records support the conclusion that NAO-like atmospheric circulation variability was the major mode responsible for the coherent variability of the investigated speleothem $\delta^{18}O$ records and more speculatively of European winter climate during the last 5 ka.

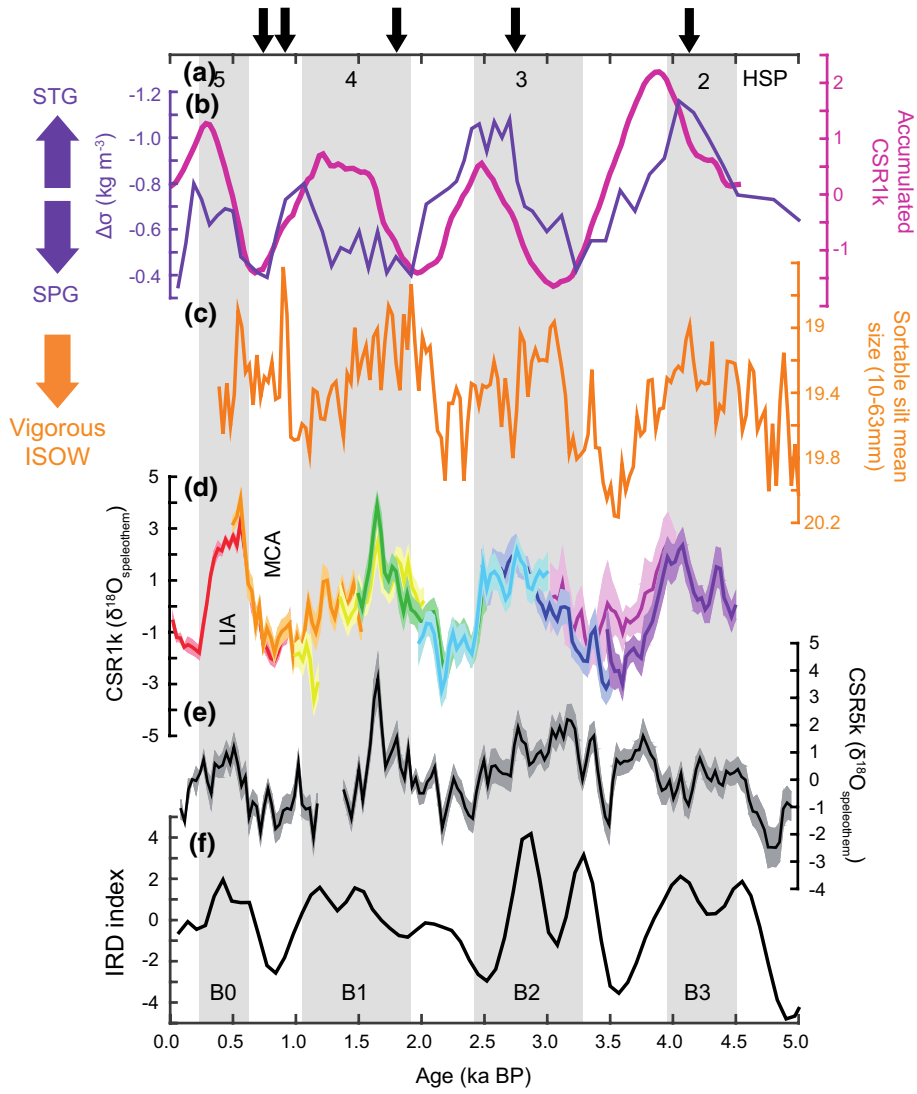

Fig. 9 Comparison of the common speleothem records (CSRs) of the 1k compilations (CSR1k) (**d**) and the 5k compilation (CSR5k) (**e**) with various records of the North Atlantic Ocean circulation history: **a** Holocene storm periods (HSP) from sediment records in coastal NW France (*grey shading vertical bars*) after Sorrel et al. (2012); the *arrows* on top indicate stormy periods inferred from the evolution of coastal dune fields in Jutland, Denmark (Clemmensen et al. 2009). These times are interpreted as stormy periods in Northern Europe associated with a negative mode of the North Atlantic Oscillation (NAO). **b** Illustration of the density difference ($\Delta\sigma$) in the upper-water-column of water south of Iceland related to the strength of the subpolar gyre (SPG). A higher density difference is caused by more saline and warmer water masses from the subtropical gyre (STG) whereas a smaller density difference is related by a greater contribution of fresh and cold water originating from the SPG. The strength of the SPG, which modulates the contribution of water masses from the STG, depends on the local wind stress (Thornalley et al. 2009). The accumulated CSR1k curve is calculated from the mean of all 1k compilations of the CSR1k records by adding the values of the mean CSR1k record from oldest to youngest together (see Figure S10 for detail). **c** The curve show the history of the strength of the Iceland Scotland Overflow Water (ISOW) retrieved by the sortable silt records from a sediment core south of Iceland. Higher values indicate a more vigorous ISOW (Mjell et al. 2015). f) Illustration of the (normalised) ice rafting debris (IRD) derived from several sediment cores in the subpolar North Atlantic that are reflecting higher occurrence of drift ice. Higher (lower) values of the IRD index denote more (less) drift ice in the subpolar North Atlantic (Bond et al. 1997, 2001) possibly related to cooler (warmer) sea surface temperatures

Furthermore, the results of the alternating westerlies are in agreement with a recent reconstruction of the western Mediterranean forest development, suggesting the development of western Mediterranean forests when the atmospheric circulation assembles NAO− like conditions (Fletcher et al. 2013). Climatic conditions favourable for forest growth in the western Mediterranean generally coincide with low lake levels in central Europe as reconstructed by Magny (2004) and Magny (2007) (see Fletcher et al. 2013 for detail). The general finding of the co-variability

Table 5 The table lists the coherent changes observed in the palaeoclimate archives compared by this study (Fig. 9) and its associated physical interpretation

CSR1k	HSP	IRD	Δσ	SMOW
Proxy observation				
↑	NAO−	↑	↑	↓
↓		↓	↓	↑
Physical interpretation				
↑	NAO−	More sea ice, cooler SSTs	Less wind stress (NAO−)	Decreased heat loss
↓		Less sea ice, warmer SSTs	More wind stress (NAO+)	Increased heat loss

This table can be used to validate model simulations in order to access if the simulations reflect the palaeoclimate observations. See also text for detail

of the compared records is summarised in Table 5 and is suitable to be used for comparisons with model simulations investigating Holocene climate variability and their forcing.

Combining all of these individual arguments, we interpret the CSR1k record to reflect changes in the mean state of the winter atmospheric circulation with predominantly southward (northward) shifted westerlies, associated with increasing (decreasing) CSR1k values. This interpretation of the CSR1k record is broadly consistent with other NAO reconstructions, suggesting a predominant negative mode of the winter NAO during the Little Ice Age and a positive winter NAO mode during the Medieval Climate Anomaly (e.g. Baker et al. 2015; Olsen et al. 2012; Trouet et al. 2009; Wassenburg et al. 2013) (Fig. 5). The differences between these NAO reconstructions, in particular between the long-term NAO reconstructions of Baker et al. (2015) and Olsen et al. (2012), and the CSR1k record can have a variety of factors: one is the compilation of used palaeoclimate records. In this study 11 speleothem records are used, whereas most of the NAO reconstruction mentioned are only based on a single palaeoclimate archives from one region. Furthermore, it is likely that changes in ocean circulation rather than the atmospheric circulation or both affect the local climates; another reason is that other atmospheric modes, like the East Atlantic (EA) pattern, can modify precipitation pattern (Comas-Bru and McDermott 2013).

The quasi-periodic alternations of northward and southward advancing westerlies, expressed by the CSR1k record, are apparently accompanied by changes in North Atlantic Ocean circulation, suggesting an enhanced (decreased) meridional heat transport for northward (southward) shifted westerlies (Mjell et al. 2015), a reduced (an enhanced) southward expansion of sea ice (Bond et al. 1997, 2001) and a stronger (weaker) SPG (Thornalley et al. 2009) for northward (southward) shifted westerlies. A recent modelling study suggests that these changes can be generated by changing the wind stress on the North Atlantic Ocean (Yang et al. 2016). Furthermore we note that the accumulated CSR1k shows a better agreement to the reconstruction of the SPG and hints that the millennial scale variability of the SPG is forced by the (accumulated) wind stress on the ocean. We stress that the CSR1k record depicts well known Holocene events of rapid climate change (4.2–3.8 ka BP; 3.5–2.5 ka BP; 1.2–1.0 ka BP; 0.6–0.15 ka BP) (Mayewski et al. 2004) suggesting that, although the research focus was here on the European continent and the North Atlantic region, the forcing of these coherent changes in the atmospheric and ocean circulation might reflect changes on a much larger scale.

6.3 Discussion of the spatio-temporal patterns of the speleothem compilations

In this section, the spatio-temporal patterns derived from the speleothem compilations and their implication for processes that cause the observed speleothem $\delta^{18}O$ variability are discussed only briefly. A detailed discussion is beyond the scope of this paper and will be presented in a subsequent publication.

Our interpretation of the CSR records implies a negative correlation to the NAO index. Therefore, to compare the spatio-temporal pattern of the individual speleothem compilations with that computed from the ECHAM5-wiso simulations (Fig. 4)—for which the 1st PC has a positive correlation to the wNAOi ($r_s = 0.42$)—either the sign of the loadings of the speleothems or that of the ECHAM5-wiso grid cells need to be inverted. For simplicity, and without loss of generality, we inverted the loadings for the ECHAM5-wiso grid cells: therefore, the loading for the grid cell of FM-3 and K-1 are positive; all others are negative.

Comparison of the spatio-temporal pattern of the 1st PC for the 5k compilation (Fig. 6) with the spatio-temporal pattern of the 1st PC retrieved from the ECHAM5-wiso model, analysing only the grid cells where investigated caves are located (Fig. 4), shows that the signs of the loading for speleothem data from the western margin (CC-3, Ireland; GAR-01, Spain) are reproduced. However, the loading disagrees for speleothem data at cave locations in the Alps (SPA-12), Germany (BU-4), Scandinavia (FM-3) and northern Turkey (SO-1). Furthermore, the strength of the coupling to the 1st PC of stalagmite SO-1 is much stronger compared with that from the model simulations.

The comparison of the spatio-temporal patterns of the 1k compilations reveal that the sign of the loadings for some speleothem $\delta^{18}O$ records is opposite compared to the loadings expected from PCA of the ECHAM5-wiso simulations (cf. Fig. 4 with Figs. 7 and 8). For example, the sign of the loading of speleothem SPA-12 is different for all 1k compilations compared to the sign of the loading computed from the model simulations.

The variation between the spatio-temporal patterns (model vs. speleothems compilations) can be explained in several ways. First, it is likely that the period simulated with the ECHAM5-wiso model is not appropriate to depict long-term mean states of the spatio-temporal pattern (42 years vs. 5 ka and 1 ka), although, the loadings for some locations reproduce quite well. Second, the quasi-periodic millennial changes of the atmospheric circulation and the ocean circulation are not likely to be fully captured by the short-term model simulations of the ECHAM5-wiso model. This might be particularly the case for cave locations where the loading between the $\delta^{18}O_{pw}$ and the 1st PC is weak (FM-3, Norway; K-1, Sweden; SO-1, Turkey; J-1, Lebanon) or where the cave is situated in a boundary region between positive and negative loadings (e.g. CC-26, Italy: cf. Fig. 3c). A recent study demonstrated also that the correlation pattern between $\delta^{18}O_{pw}$ and the wNAOi in Europe is affected by 2nd order modes of the variability of the atmospheric circulation in some regions of Europe (Comas-Bru et al. 2016) and this may provide part of the explanation. However, notwithstanding these limitations, the spatio-temporal pattern of the 1st PC of the ECHAM5-wiso $\delta^{18}O_{pw}$ simulations—which is forced by the modern-day winter mode of the NAO – can yield important insights into the processes that determine speleothem $\delta^{18}O$ variability. When the sign of a loading of the ECHAM5-wiso simulations is reproduced by the loading of the speleothem MC-PCA, it suggests that the speleothem $\delta^{18}O$ variability can be caused by variations in $\delta^{18}O_{pw}$ and when they disagree it indicates that other processes, acting on a local scale, are mainly responsible for the speleothem $\delta^{18}O$ variability. Regional scale climate processes are unlikely to change the sign of the loading and so local-scale processes are only considered in the following discussion. Among these local-scale processes, isotope disequilibrium effects (Deininger et al. 2012; Mühlinghaus et al. 2009) can change the spatio-temporal pattern of the dominant mode of $\delta^{18}O_{pw}$ variability by changes in some the cave-specific parameters.

In this study the observed differences between the spatio-temporal pattern of the dominant mode of the speleothem $\delta^{18}O$ compilations and the ECHAM5-wiso model is explored by focusing on some cave sites as examples. In the first example we consider the speleothem SPA-12 (Austria) for which a different sign of the loading is observed for all compilations. This suggests that the determining variable of these speleothem $\delta^{18}O$ records is not the $\delta^{18}O_{pw}$ signal, but rather a cave specific parameter (e.g. air temperature); notwithstanding the tight coupling of data from these sites to the dominant mode responsible for observed coherency. The opposite sign of the speleothem loading suggest that the speleothem $\delta^{18}O$ record is inverted compared with the $\delta^{18}O_{pw}$ signal expected from the dominant mode. To invert an increasing (decreasing) $\delta^{18}O_{pw}$ signal, the cave air temperature must increase (decrease) and the other cave parameters (drip interval, cave air CO_2 concentration associated with the cave ventilation and super-saturation of the cave drip water) must decrease (increase) (Deininger et al. 2012).

While cave parameters such as the super-saturation of the drip water and cave ventilation are likely determined by local factors (e.g. cave topography), air temperature and drip intervals are cave parameters whose long-term variability could be coupled to the long-term variability in temperature and precipitation determined by the dominant mode. From modern day reanalysis data it is known that winter air temperature increase (decrease) in the Alps for NAO+ (NAO−) modes (e.g. Comas-Bru and McDermott 2013). If the millennial shifts of the westerlies cause similar temperature variations in the Alps as the NAO does, the cave air temperature can be warmer for northward shifted westerlies and cooler for southward shifted westerlies. This temperature-mechanism would cause a speleothem $\delta^{18}O$ change in the opposite direction to that expected from $\delta^{18}O_{pw}$ variations, and could therefore explain the opposite loadings for the speleothems SPA-12. This conclusion is in agreement with the study of Mangini et al. (2005) who argued that the $\delta^{18}O$ record of SPA-12 is temperature dominated during the last 2 ka; our study suggests that this might be even the case for the last 4.5 ka.

Another example is stalagmite BU-4 (Germany) whose loading agrees with the sign expected from the ECHAM5-wiso model for compilation 1k.I–1k.V (4.5–1.5 ka BP) and disagrees for compilation 5k and compilation 1k.VI, 1k.VII and 1k.VIII (2.0–0.01 ka BP). This suggests that for the time slices covering the period from 4.5 to 1.5 ka BP (compilation 1k.I–1k.V) the $\delta^{18}O$ record of BU-4 is dominated by the $\delta^{18}O_{pw}$ signal but that the $\delta^{18}O$ record of BU-4 is driven by cave specific parameter (e.g. temperature) from 2.0 to 0.01 ka BP (compilation 1k.VI–1k.VIII) inverting the $\delta^{18}O_{pw}$ signal. It is reasonable to assume similar relationships between temperature for Bunker Cave in Germany as for the previously discussed cave systems of SPA-12. Hence, the inversion of the sign of the loading of BU-4 between the compilations 1k.V (2.5–1.5 ka BP) and 1k.VI (2.0–1.0 ka BP) suggests that the determining factors controlling BU-4s $\delta^{18}O$ record have changed. Similar explanations can be introduced for loadings for speleothems of compilations, where the loading of the speleothem has an

opposite sign compared to the loading derived from the ECHAM5-wiso model. To test the conclusions derived from the changes of the spatio-temporal patterns, independent speleothem based temperature-sensitive proxy-analysis (e.g. Meckler et al. 2015) or analysis of fluid inclusion $\delta^{18}O$ values (e.g. Labuhn et al. 2015) could provide additional information on past $\delta^{18}O_{pw}$ changes.

While our approach highlights coherent variability in speleothem $\delta^{18}O$ records for the last 4.5 ka, several limitations remain. Chief among these is that while the spatial coverage of speleothem $\delta^{18}O$ records within Europe with the required chronological control and sampling resolution is good compared with many regions globally, it is still inadequate to assess important questions such as the role of north–south (NAO-related) variability versus west-east variability. A recent study that compares the correlation of two European speleothems geochemical proxy indicates that the NAO has reorganised in the Early Holocene (between 9 and 8 ka BP) due primarily to the retreat of the Laurentide ice sheet (Wassenburg et al. 2016) further highlighting that coherent changes of the state of the NAO can influence speleothem geochemical proxy and their spatio-temporal coherence. The present indications for the last 4.5 ka are that a west to east switch in the sign of correlations between individual sites and the CSR prevail (Figs. 6, 7, 8), reminiscent of the cross-over in the long-term trends in Holocene speleothem $\delta^{18}O$ records from the western margin into central Europe reconstructed by McDermott et al. (2011). Further evaluation of these important questions will require better spatial and temporal coverage in the speleothem $\delta^{18}O$ datasets. In addition inter-comparisons with independent climate reconstructions, with model outputs simulating past $\delta^{18}O_{pw}$ pattern as well as direct measurements of meteoric water $\delta^{18}O$ through speleothem fluid inclusion analyses are clearly required to further test these possibilities. A detailed discussion of the spatio-temporal pattern will be subject of a subsequent publication.

7 Summary

Statistical methods for analysing spatio-temporal changes of palaeoclimate archives are still rather underdeveloped. This is mainly owing to inherent difficult data properties, such as age uncertainties, persistence and unevenly spaced climate-proxy records. Further research is therefore necessary to explore the full potential of these techniques, such as simulations with artificial time series in order to quantitatively examine the performance of statistical tools (Mudelsee 2014). The present study is a contribution towards these aims applying, in contrast to other studies (e.g. Rehfeld et al. 2013), an adaptation of Principal Component Analysis (PCA) that accounts for age uncertainties in unequally spaced climate-proxy records using a Monte Carlo approach (MC-PCA).

We performed, for the first time, a spatio-temporal coherency analysis of European speleothem $\delta^{18}O$ records during the last 5 ka using the MC-PCA approach. A total of 11 speleothem $\delta^{18}O$ records was analysed that cover most of the European continent, with the exception of the Mediterranean region, ranging from the European western margin to Northern Turkey and Lebanon and from the Alps to Scandinavia. Based on the results of the MC-PCA, common speleothem records (CSR5k, CSR1k) were constructed from the derived leading mode of the investigated speleothem compilations. This results demonstrate that the investigated speleothem $\delta^{18}O$ records have imprinted a common European-scale climate-related signal depicting a millennial cyclicity that was also reported by Mangini et al. (2007) for a composite speleothem record from Spannagel cave (Austria). Our study suggests that this millennial cyclicity is not only a mode of speleothem $\delta^{18}O$ variability for this single cave site but for European speleothems in general. These changes are imprinted in the speleothem $\delta^{18}O$ records via the $\delta^{18}O_{pw}$ signal and possible oxygen isotope disequilibrium effects—superimposed by local site-specific signals.

The good agreement between the CSR1k as well as accumulated CSR1k record and independent sedimentary records of the history of the Atlantic subpolar gyre (SPG), the ocean stacked North Atlantic IRD index, the vigour of the ISOW and late Holocene storm periods during the last 5 ka suggests that similar climate mechanisms are responsible for the variability of the strength of these records and European winter climate variability recorded by the speleothem records. A recent study has identified that these changes can be forced by changes of the wind stress on the ocean (Yang et al. 2016), indicating the alternating northward (increased wind stress) and southward (decreased wind stress) shifting westerlies—expressed by the CSR1k record—can trigger this oceanic variability. Furthermore, this study hints that the strength of the SPG is forced by wind stress as suggested by (Thornalley et al. 2009). Similar conclusions where made for the transition from the mid to the late Holocene (Colin et al. 2010; Morley et al. 2014). We conclude therefore that a possible driver could be a behaviour of the atmospheric circulation with northward and southward propagating westerlies (eventually akin to that of the NAO but on millennial instead if decadal time scales), respectively. However, the ultimate driver for this oscillation in the meridional position of the westerlies remains unclear. Finally, we note, that the proposed mechanism for the late Holocene millennial variability needs to be further investigated by model simulations and additional palaeoclimate proxy records, for example, the effect of the millennial climate variation on the vigour of the North Atlantic Deep Water (NADW).

Acknowledgments We thank the executive editor Jean-Claude Duplessy, Jud Partin and three anonymous reviewers for their constructive comments that significantly improved the manuscript. M.D. developed the MC-PCA approach for speleothems during his Ph.D. at the Institute of Environmental Physics of the Heidelberg University, Germany, which was funded by the Deutsche Forschungsgemeinschaft (DFG) research group "DAPHNE" (DFG Forschergruppe 668). He is currently funded by the Irish Research Council (IRC) by a Government of Ireland Postdoctoral Fellowship (GOIPD/2015/789). F.McD. acknowledges support from Science Foundation Ireland through its Research Frontiers Programme (RFP) Grants 07/RFP/GEOF265 and 08/FRP/GEO1184. The MATLAB code for the MC-PCA approach is available from the authors.

References

Anchukaitis KJ, Tierney JE (2012) Identifying coherent spatiotemporal modes in time-uncertain proxy paleoclimate records. Clim Dyn 41:1291–1306

Baker A, Genty D, Dreybrodt W, Barnes WL, Mockler NJ, Grapes J (1998) Testing theoretically predicted stalagmite growth rate with recent annually laminated samples: implications for past stalagmite deposition. Geochim Cosmochim Acta 62:393–404

Baker A, Wilson R, Fairchild IJ, Franke J, Spötl C, Mattey D, Trouet V, Fuller L (2011) High resolution δ 18 O and δ 13 C records from an annually laminated Scottish stalagmite and relationship with last millennium climate. Global Planet Change 79:303–311

Baker A, Hellstrom C, Kelly BF, Mariethoz G, Trouet V (2015) A composite annual-resolution stalagmite record of North Atlantic climate over the last three millennia. Sci Rep 5:10307

Baldini LM, McDermott F, Foley AM, Baldini JUL (2008) Spatial variability in the European winter precipitation δ18O-NAO relationship: implications for reconstructing NAO-mode climate variability in the Holocene. Geophys Res Lett 35:L04709–L04709

Baldini LM, McDermott F, Baldini JUL, Arias P, Cueto M, Fairchild IJ, Hoffmann DL, Mattey DP, Müller W, Nita DC, Ontañón R, Garciá-Moncó C, Richards DA (2015) Regional temperature, atmospheric circulation, and sea-ice variability within the Younger Dryas Event constrained using a speleothem from northern Iberia. Earth Planet Sci Lett 419:101–110

Blindheim J, Østerhus S (2005) The Nordic Seas, main oceanographic features. An integrated perspective, The Nordic seas, pp 11–37

Bond G, Showers W, Cheseby M, Lotti R, Almasi P, Priore P, Cullen H, Hajdas I, Bonani G (1997) A pervasive millennial-scale cycle in North Atlantic Holocene and glacial climates. Science 278:1257–1266

Bond G, Kromer B, Beer J, Muscheler R, Evans MN, Showers W, Hoffmann S, Lotti-Bond R, Hajdas I, Bonani G (2001) Persistent solar influence on North Atlantic climate during the Holocene. Science 294:2130–2136

Cattell RB (1966) The scree test for the number of factors. Multivar Behav Res 1:245–276

Cheng H, Lawrence Edwards R, Shen C-C, Polyak VJ, Asmerom Y, Woodhead J, Hellstrom J, Wang Y, Kong X, Spötl C, Wang X, Calvin Alexander E Jr (2013) Improvements in 230Th dating, 230Th and 234U half-life values, and U–Th isotopic measurements by multi-collector inductively coupled plasma mass spectrometry. Earth Planet Sci Lett 371–372:82–91

Cheng H, Sinha A, Verheyden S, Nader FH, Li XL, Zhang PZ, Yin JJ, Yi L, Peng YB, Rao ZG (2015) The climate variability in northern Levant over the past 20,000 years. Geophys Res Lett 42:8641–8650

Clemmensen LB, Murray A, Heinemeier J, de Jong R (2009) The evolution of Holocene coastal dunefields, Jutland, Denmark: a record of climate change over the past 5000 years. Geomorphology 105:303–313

Colin C, Frank N, Copard K, Douville E (2010) Neodymium isotopic composition of deep-sea corals from the NE Atlantic: implications for past hydrological changes during the Holocene. Quat Sci Rev 29:2509–2517

Comas-Bru L, McDermott F (2013) Impacts of the EA and SCA patterns on the European twentieth century NAO-winter climate relationship. Q J R Meteorol Soc 140:354–363

Comas-Bru L, McDermott F, Werner M (2016) The effect of the East Atlantic pattern on the precipitation δ18O-NAO relationship in Europe. Clim Dyn 47:2059–2069

Copard K, Colin C, Henderson GM, Scholten J, Douville E, Sicre MA, Frank N (2012) Late Holocene intermediate water variability in the northeastern Atlantic as recorded by deep-sea corals. Earth Planet Sci Lett 313:34–44

Day CC, Henderson GM (2011) Oxygen isotopes in calcite grown under cave-analogue conditions. Geochim Cosmochim Acta 75:3956–3972

Deininger M (2013) The European holocene climate from the Speleothem's view, PhD thesis. Department of Physics and Astronomy, Faculty of Physics and Astronomy, University of Heidelberg. http://www.ub.uni-heidelberg.de/archiv/16039, http://www.ub.uni-heidelberg.de/archiv/16039

Deininger M, Fohlmeister J, Scholz D, Mangini A (2012) Isotope disequilibrium effects: the influence of evaporation and ventilation effects on the carbon and oxygen isotope composition of speleothems—a model approach. Geochim Cosmochim Acta 96:57–79

Dietrich S, Werner M, Spangehl T, Lohmann G (2013) Influence of orbital forcing and solar activity on water isotopes in precipitation during the mid-and late Holocene. Clim Past 9:13–26. doi:10.5194/cp-9-13-2013

Dreybrodt W, Scholz D (2011) Climatic dependence of stable carbon and oxygen isotope signals recorded in speleothems: from soil water to speleothem calcite. Geochim Cosmochim Acta 75:734–752

Fairchild IJ, Treble PC (2009) Trace elements in speleothems as recorders of environmental change. Quat Sci Rev 28:449–468

Fairchild IJ, Smith CL, Baker A, Fuller L, Spötl C, Mattey D, McDermott F (2006) Modification and preservation of environmental signals in speleothems. Earth Sci Rev 75:105–153

Feldhoff JH, Donner RV, Donges JF, Marwan N, Kurths J (2012) Geometric detection of coupling directions by means of inter-system recurrence networks. Phys Lett A 376:3504–3513

Field RD (2010) Observed and modeled controls on precipitation δ18O over Europe: from local temperature to the Northern Annular Mode. J Geophys Res Atmos 1984–2012:115

Fischer MJ (2016) Predictable components in global speleothem δ 18 O. Quat Sci Rev 131:380–392

Fletcher WJ, Debret M, Goñi MFS (2013) Mid-Holocene emergence of a low-frequency millennial oscillation in western Mediterranean climate: implications for past dynamics of the North Atlantic atmospheric westerlies. Holocene. doi:10.1177/0959683612460783

Fleitmann D, Cheng H, Badertscher S, Edwards RL, Mudelsee M, Göktürk OM, Fankhauser A, Pickering R, Raible CC, Matter A, Kramers JD, Tuysuz O (2009) Timing and climatic impact of Greenland interstadials recorded in stalagmites from northern Turkey. Geophys Res Lett. doi:10.1029/2009GL040050

Fohlmeister J, Schröder-Ritzrau A, Scholz D, Spöotl C, Riechelmann DFC, Mudelsee M, Wackerbarth A, Gerdes A, Riechelmann S, Immenhauser A, Richter DK, Mangini A (2012) Bunker Cave stalagmites: an archive for central European Holocene climate variability. Clim Past 8(5):1751–1764. doi:10.5194/cp-8-1751-2012

Frisia S, Borsato A, Fairchild IJ, McDermott F (2000) Calcite fabrics, growth mechanisms, and environments of formation in speleothems from the Italian Alps and southwestern Ireland. J Sediment Res 70:1183–1196

Göktürk OM, Fleitmann D, Badertscher S, Cheng H, Edwards RL, Leuenberger M, Fankhauser A, Tüysüz O, Kramers J (2011) Climate on the southern Black Sea coast during the Holocene: implications from the Sofular Cave record. Quat Sci Rev 30:2433–2445

Grinsted A, Moore JC, Jevrejeva S (2004) Application of the cross wavelet transform and wavelet coherence to geophysical time series. Nonlinear Process Geophys 11:561–566

Hartland A, Fairchild IJ, Lead JR, Borsato A, Baker A, Frisia S, Baalousha M (2012) From soil to cave: transport of trace metals by natural organic matter in karst dripwaters. Chem Geol 304:68–82

Hoffmann DL, Prytulak J, Richards DA, Elliott T, Coath CD, Smart PL, Scholz D (2007) Procedures for accurate U and Th isotope measurements by high precision MC-ICPMS. Int J Mass Spectrom 264:97–109

Huang Y, Fairchild IJ (2001) Partitioning of Sr2+ and Mg2+ into calcite under karst-analogue experimental conditions. Geochim Cosmochim Acta 65:47–62

Hurrell JW (1995) Decadal trends in the North-Atlantic oscillation—regional temperatures and precipitation. Science 269:676–679

Jex CN, Phipps SJ, Baker A, Bradley C (2013) Reducing uncertainty in the climatic interpretations of speleothem δ18O. Geophys Res Lett 40:2259–2264

Kaiser HF (1960) The application of electronic-computers to factor-analysis. Educ Psychol Meas 20:141–151

Labuhn I, Genty D, Vonhof H, Bourdin C, Blamart D, Douville E, Ruan J, Cheng H, Edwards RL, Pons-Branchu E, Pierre M (2015) A high-resolution fluid inclusion δ18O record from a stalagmite in SW France: modern calibration and comparison with multiple proxies. Quat Sci Rev 110:152–165

Lachniet MS (2009) Climatic and environmental controls on speleothem oxygen-isotope values. Quat Sci Rev 28:412–432

Lachniet MS, Patterson WP, Burns S, Asmerom Y, Polyak V (2007) Caribbean and Pacific moisture sources on the Isthmus of Panama revealed from stalagmite and surface water δ18O gradients. Geophys Res Lett 34:L01708. doi:10.1029/2006GL028469

Lamb HH (2002) Climate, history and the modern world. Routledge, New York

Langebroek PM, Werner M, Lohmann G (2011) Climate information imprinted in oxygen-isotopic composition of precipitation in Europe. Earth Planet Sci Lett 311:144–154

Linge H, Lauritzen SE, Andersson C, Hansen JK, Skoglund RØ, Sundqvist HS (2009) Stable isotope records for the last 10 000 years from Okshola cave (Fauske, northern Norway) and regional comparisons. Clim Past 5:667–682

Lohmann G, Wackerbarth A, Langebroek PM, Werner M, Fohlmeister J, Scholz D, Mangini A (2013) Simulated European stalagmite record and its relation to a quasi-decadal climate mode. Clim Past 9:89–98

Luetscher M, Hoffmann DL, Frisia S, Spötl C (2011) Holocene glacier history from alpine speleothems, Milchbach cave, Switzerland. Earth Planet Sci Letters 302:95–106

Magny M (2004) Holocene climate variability as reflected by mid-European lake-level fluctuations and its probable impact on prehistoric human settlements. Quat Int 113:65–79

Magny M (2007) Holocene fluctuations of lake levels in west-central Europe: methods of reconstruction, regional pattern, palaeoclimatic significance and forcing factors. Encyclop Quat Sci 1389–1399

Mangini A, Spötl C, Verdes P (2005) Reconstruction of temperature in the Central Alps during the past 2000 yr from a δ 18 O stalagmite record. Earth Planet Sci Lett 235:741–751

Mangini A, Verdes P, Spötl C, Scholz D, Vollweiler N, Kromer B (2007) Persistent influence of the North Atlantic hydrography on central European winter temperature during the last 9000 years. Geophys Res Lett 34:L02704

Mann ME, Bradley RS, Hughes MK (1998) Global-scale temperature patterns and climate forcing over the past six centuries. Nature 392:779–787

Marshall J, Johnson H, Goodman J (2001) A study of the interaction of the North Atlantic Oscillation with ocean circulation. J Clim 14:1399–1421

Mayewski PA, Rohling EE, Curt Stager J, Karlén W, Maasch KA, David Meeker L, Meyerson EA, Gasse F, van Kreveld S, Holmgren K (2004) Holocene climate variability. Quat Res 62:243–255

McCarthy GD, Haigh ID, Hirschi JJM, Grist JP, Smeed DA (2015) Ocean impact on decadal Atlantic climate variability revealed by sea-level observations. Nature 521:508–510

McDermott F (2004) Palaeo-climate reconstruction from stable isotope variations in speleothems: a review. Quat Sci Rev 23:901–918

McDermott F, Frisia S, Huang Y, Longinelli A, Spiro B, Heaton THE, Hawkesworth CJ, Borsato A, Keppens E, Fairchild IJ et al (1999) Holocene climate variability in Europe: evidence from δ 18 O, textural and extension-rate variations in three speleothems. Quat Sci Rev 18:1021–1038

McDermott F, Mattey DP, Hawkesworth C (2001) Centennial-scale Holocene climate variability revealed by a high-resolution speleothem δ18O record from SW Ireland. Science 294:1328–1331

McDermott F, Atkinson TC, Fairchild IJ, Baldini LM, Mattey DP (2011) A first evaluation of the spatial gradients in δ18O recorded by European Holocene speleothems. Global Planet Change 79:275–287

Meckler AN, Affolter S, Dublyansky YV, Krüger Y, Vogel N, Bernasconi SM, Frenz M, Kipfer R, Leuenberger M, Spötl C (2015) Glacial–interglacial temperature change in the tropical West Pacific: a comparison of stalagmite-based paleo-thermometers. Quat Sci Rev 127:90–116

Mischel SA, Scholz D, Spötl C (2015) δ18O values of cave drip water: a promising proxy for the reconstruction of the North Atlantic Oscillation? Clim Dyn 45:3035–3050

Mjell TL, Ninnemann US, Eldevik T, Kleiven HKF (2015) Holocene multidecadal-to millennial-scale variations in Iceland–Scotland overflow and their relationship to climate. Paleoceanography 30:558–569

Moreno-Chamarro E, Zanchettin D, Lohmann K, Jungclaus JH (2016) An abrupt weakening of the subpolar gyre as trigger of Little Ice Age-type episodes. Clim Dyn. doi:10.1007/s00382-016-3106-7

Morley A, Rosenthal Y, deMenocal P (2014) Ocean–atmosphere climate shift during the mid-to-late Holocene transition. Earth Planet Sci Lett 388:18–26

Mudelsee M (2014) Climate time series analysis: classical statistical and bootstrap methods, 2nd edn. Springer, Dordrecht

Mühlinghaus C, Scholz D, Mangini A (2009) Modelling fractionation of stable isotopes in stalagmites. Geochim Cosmochim Acta 73:7275–7289

North GR, Bell TL, Cahalan RF, Moeng FJ (1982) Sampling errors in the estimation of empirical orthogonal functions. Mon Weather Rev 110:699–706

Olsen J, Anderson NJ, Knudsen MF (2012) Variability of the North Atlantic Oscillation over the past 5,200 years. Nat Geosci 5:808–812

Polag D, Scholz D, Mühlinghaus C, Spötl C, Schröder-Ritzrau A, Segl M, Mangini A (2010) Stable isotope fractionation in speleothems: laboratory experiments. Chem Geol 279:31–39

Preisendorfer RW (1988) Principal component analysis in meteorology and oceanography. Elsevier, Amsterdam

Rehfeld K, Marwan N, Heitzig J, Kurths J (2011) Comparison of correlation analysis techniques for irregularly sampled time series. Nonlinear Process Geophys 18:389–404

Rehfeld K, Marwan N, Breitenbach SFM, Kurths J (2013) Late Holocene Asian summer monsoon dynamics from small but complex networks of paleoclimate data. Clim Dyn 41:3–19

Richards DA, Dorale JA (2003) Uranium-series chronology and environmental applications of speleothems. Rev Mineral Geochem 52:407–460

Riechelmann DFC, Deininger M, Scholz D, Riechelmann S, Schröder-Ritzrau A, Spötl C, Richter DK, Mangini A, Immenhauser A (2013) Disequilibrium carbon and oxygen isotope fractionation in recent cave calcite: comparison of cave precipitates and model data. Geochim Cosmochim Acta 103:232–244

Scholz D, Hoffmann DL (2011) StalAge—an algorithm designed for construction of speleothem age models. Quat Geochronol 6:369–382

Sorrel P, Debret M, Billeaud I, Jaccard SL, McManus JF, Tessier B (2012) Persistent non-solar forcing of Holocene storm dynamics in coastal sedimentary archives. Nat Geosci 5:892–896

Spötl C, Mattey D (2006) Stable isotope microsampling of speleothems for palaeoenvironmental studies: a comparison of microdrill, micromill and laser ablation techniques. Chem Geol 235:48–58

Sundqvist HS, Holmgren K, Moberg A, Spoetl C, Mangini A, (2010) Stable isotopes in a stalagmite from NW Sweden document environmental changes over the past 4000 years. Boreas 39:77–86

Thornalley DJR, Elderfield H, McCave IN (2009) Holocene oscillations in temperature and salinity of the surface subpolar North Atlantic. Nature 457:711–714

Tremaine DM, Froelich PN, Wang Y (2011) Speleothem calcite farmed in situ: modern calibration of δ18O and δ13C paleoclimate proxies in a continuously-monitored natural cave system. Geochim Cosmochim Acta 75:4929–4950

Trouet V, Esper J, Graham NE, Baker A, Scourse JD, Frank DC (2009) Persistent positive North Atlantic Oscillation mode dominated the medieval climate anomaly. Science 324:78–80

Visbeck M, Chassignet EP, Curry RG, Delworth TL, Dickson RR, Krahmann G (2003) The ocean's response to North Atlantic Oscillation variability. In: The North Atlantic Oscillation: climatic significance and environmental impact, pp 113–145

Wallace JM, Gutzler DS (1981) Teleconnections in the geopotential height field during the northern hemisphere winter. Mon Weather Rev 109:784

Wassenburg JA, Immenhauser A, Richter DK, Niedermayr A, Riechelmann S, Fietzke J, Scholz D, Jochum KP, Fohlmeister J, Schroder-Ritzrau A, Sabaoui A, Riechelmann DFC, Schneider L, Esper J (2013) Moroccan speleothem and tree ring records suggest a variable positive state of the North Atlantic Oscillation during the Medieval Warm Period. Earth Planet Sci Lett 375:291–302

Wassenburg JA, Dietrich S, Fietzke J, Fohlmeister J, Jochum KP, Scholz D, Richter DK, Sabaoui A, Spötl C, Lohmann G (2016) Reorganization of the North Atlantic Oscillation during early Holocene deglaciation. Nat Geosci 9:602–605. doi:10.1038/ngeo2767

Werner M, Langebroek PM, Carlsen T, Herold M, Lohmann G (2011) Stable water isotopes in the ECHAM5 general circulation model: toward high-resolution isotope modeling on a global scale. J Geophys Res 116:D15109–D15109

Yang H, Wang K, Dai H, Wang Y, Li Q (2016) Wind effect on the Atlantic meridional overturning circulation via sea ice and vertical diffusion. Clim Dyn 46:3387–3403

Zanchetta G, Drysdale RN, Hellstrom JC, Fallick AE, Isola I, Gagan MK, Pareschi MT (2007) Enhanced rainfall in the Western Mediterranean during deposition of sapropel S1: stalagmite evidence from Corchia cave (Central Italy). Quat Sci Rev 26:279–286